Xiang *et al. Stem Cell Research & Therapy* (2024) 15:462
https://doi.org/10.1186/s13287-024-04069-5

Stem Cell Research & Therapy

RESEARCH

Open Access

Exosomes derived from minor salivary gland mesenchymal stem cells: a promising novel exosome exhibiting pro-angiogenic and wound healing effects similar to those of adipose-derived stem cell exosomes

Haibo Xiang[1†], Pengbing Ding[1†], Jiaying Qian[1], Enhang Lu[1], Yimou Sun[1], Seyeon Lee[2], Zhenkun Zhao[1], Zhixuan Sun[1] and Zhenmin Zhao[1*]

Abstract

Backgrounds Minor salivary gland mesenchymal stem cells (MSGMSCs) can be easily extracted and have a broad range of sources. Applying exosomes to wounds is a highly promising method for promoting wound healing. Exosomes derived from different stem cell types have been proven to enhance wound healing, with adipose-derived stem cell (ADSC)-derived exosomes being the most extensively researched. Considering that MSGMSCs have advantages such as easier extraction compared to ADSCs, MSGMSCs should also be a very promising type of stem cell in exosome therapy. However, whether MSGMSC-derived exosomes (MSGMSC-exos) can promote wound healing and how they compare to ADSC-derived exosomes (ADSC-exos) in the wound healing process remain unclear.

Materials The effects of MSGMSC-exos and ADSC-exos on angiogenesis in wound healing were investigated in vitro using CCK-8, scratch assays, and tube formation assays. Subsequently, the promotion of wound healing by MSGMSC-exos and ADSC-exos was evaluated in vivo using a full-thickness wound defect model in mice. Immunohistochemistry was used to verify the effects of MSGMSC-exos and ADSC-exos on promoting collagen deposition, angiogenesis, and cell proliferation in the wound. Immunofluorescence staining was performed to investigate the role of MSGMSC-exos and ADSC-exos in modulating the inflammatory response in the wound. Furthermore, proteomic sequencing was conducted to investigate the functional similarities and differences between the proteomes of MSGMSC-exos and ADSC-exos, with key protein contents verified by ELISA.

Results MSGMSC-exos exhibited similar effects as ADSC-exos in promoting the migration, proliferation, and tube formation of human umbilical vein endothelial cells (HUVECs) in vitro, with a comparable dose-dependent effect. In vivo experiments confirmed that MSGMSC-exos have similar wound healing-promoting functions as ADSC-exos. MSGMSC-exos promoted the neovascularization and maturation of blood vessels in vivo at a level comparable to ADSC-exos. Despite MSGMSC-exos showing less collagen deposition than ADSC-exos, they exhibited stronger

[†]Haibo Xiang and Pengbing Ding contributed equally to this work and are co-first authors.

*Correspondence:
Zhenmin Zhao
zzmbysy@sina.com
Full list of author information is available at the end of the article

anti-scar formation and anti-inflammatory effects. Proteomic analysis revealed that the proteins promoting wound healing in both MSGMSC-exos and ADSC-exos were relatively conserved, with ITGB1 identified as a critical protein for angiogenesis. Further differential analysis revealed that the functions specifically enriched in MSGMSC-exos and ADSC-exos reflected the functions of their source tissue.

Conclusions Our study confirms that MSGMSC-exos exhibit highly similar wound healing and angiogenesis-promoting functions compared to ADSC-exos, and the proteins involved in promoting wound healing in both are relatively conserved. Moreover, MSGMSC-exos show stronger anti-scar formation and anti-inflammatory effects than ADSC-exos. This suggests that MSGMSCs are a promising stem cell source with broad applications in wound healing treatment.

Keywords Exosome therapy, Wound healing, Human minor salivary mesenchymal stem cells, Adipose-derived stem cells

Background

Skin is the largest organ of the human body, playing an essential role in protecting us from physical trauma, thermal injury, UV radiation, and infections caused by external pathogens [1]. Meanwhile, skin is susceptible to damage due to its exposure. Injuries like cuts, slashes, burns, or abrasions can breach the protective barrier and result in skin wounds. Skin wound management is a vital topic in medicine since ineffective skin wound healing increases the morbidity and mortality rate and is a severe burden of both harmed individuals and the whole society [2, 3]. Traditional therapies for wounds include debridement, skin grafting, negative pressure wound therapy, tissue expansion, and various wound closure techniques [4, 5]. However, these therapies may sometimes inefficacious due to impaired cell function and the pathological conditions of wound sites [6]. Therefore, exploring methods to enhance the wound healing process is a crucial clinical objective. Against this backdrop, exosomes derived from variety types of stem cells have captured the attention of researchers due to their biocompatibility and cell-free approach [7, 8]. The validity of utilizing diverse exosome types, including those sourced from adipose-derived stem cells (ADSCs), bone marrow-derived stem cells (BMSCs), Umbilical cord derived stem cells (UCSCs) and epidermal stem cells (ESCs), in enhancing wound healing has been verified [9–15]. Among these stem cells, exosomes derived from ADSC (ADSC-exos) are the most extensively studied due to the abundant distribution and endocrine function of adipose tissue [16]. Up to now, it has been universally acknowledged that ADSC-exos exert a favorable impact on wound healing and hold significant promise for future therapeutic applications [17, 18].

The wound healing primarily consists of four stages: hemostasis, inflammation, proliferation, and remodeling. Angiogenesis plays an indispensable role in orchestrating the intricate symphony of wound healing across these 4 stages for the following reasons: (1) The newly formed vascular can facilitate the delivery of oxygen and micronutrients to the wound bed, ensuring the tissue growth and concurrently aiding in the removal of catabolic waste products [19, 20]. (2) Adequate angiogenesis facilitates the migration of various cell types, including immune cells and fibroblasts, to the wound site. This serves a dual function of safeguarding the wound against potential infections while actively participating in the processes of tissue regeneration and remodeling [21, 22]. ADSC-exos have been conclusively demonstrated to positively influence the proliferation and migration of vascular endothelial cells, thereby enhancing angiogenesis during wound healing [23]. Moreover, various subclasses of miRNAs related to angiogenesis (miR-125a, miR-31, miR-21, miR-126, miR-130a) carried by ADSC-exos have been proven to contribute to promoting wound healing by increasing angiogenesis [24–28]. However, liposuction for obtaining ADSCs is invasive and associated with risks such as infection, bruising and swelling, irregular contours and scarring [29]. Additionally, extracting ADSCs is a complicated and inefficient process, consuming a significant amount of effort [30]. More research should be conducted to discover a new type of stem cell that is easily accessible and causes less pain.

Saliva contains various bioactive components such as growth factors and antimicrobial peptides, which have been proven to promote wound healing [31, 32]. Therefore, we speculate that the secretome of salivary gland stem cells might play a role in promoting wound healing. As previously discussed, we aim to find a new type of stem cell that is easy to obtain, widely available, and presents fewer post-extraction complications. The minor salivary glands, which are commonly located in the oral submucosa, have become an ideal source. The minor salivary glands are widely distributed in the oral submucosa and are easily accessible. Furthermore, a typical individual has approximately 800 to 1,000 minor salivary glands, providing a broad source [33]. Our team has successfully extracted minor salivary gland mesenchymal stem cells (MSGMSCs) from minor salivary gland tissue and

demonstrated their stem cell properties [34–36]. MSGMSCs originate from oral tissue, which exhibits rapid regeneration following extraction and results in less pain and fewer scars compared to liposuction. Meanwhile, compared to ADSCs, MSGMSCs need smaller amount of tissue to obtain an equivalent number of primary cells, and the extraction process of MSGMSCs is rather simple [35]. An in vitro study demonstrates that MSGMSC can be cultured for up to 20 passages without obvious morphological changes and retains the ability for self-renewal [34]. MSGMSCs have a promising future in the application of stem cell therapy considering the characteristics discussed above. Given the widely acknowledged positive effects of ADSC-exos on angiogenesis and wound healing, our study aims to investigate whether MSGMSC-exos can similarly enhance angiogenesis and wound healing, and to compare the effectiveness of MSGMSC-exos with that of ADSC-exos.

Materials and methods

Cell culture and characterization

The extraction of ADSCs and MSGMSCs was described before [34, 37]. ADSCs and MSGMSCs were cultured in 75 cm^2 culture dish (353024; Corning, America) with Dulbecco's modified Eagle's medium (DMEM)-low glucose (SH30021.01; HyClone, America) supplemented with 10% fetal bovine serum (FBS) (10100; Gibco, America), 100 U/ml penicillin and 100 μg/ml streptomycin (SV30010; HyClone, America). Both cells were incubated in a CO_2-regulated incubator within a humidified 95% air and 5% CO_2 atmosphere. The culture media were replaced every 2 days. The cells were passaged after reaching 80 percent confluence and cells at 3–6 passages were used for further extraction of exosomes.

To evaluate the differentiation potential of ADSCs and MSGMSCs, adipogenic, osteogenic, and chondrogenic induction were performed. Flow cytometry was performed to determine the expression of HLA-DR, CD11b, CD14, CD29, CD105, and CD166.

Extraction and identification of ADSC-exos and MSGMSC-exos

The 3–6 passages of ADSCs and MSGMSCs were proliferated to approximately 70 percent of confluent and then cultured in MSC NutriStem® XF Medium (05–200-1A; Biological Industry, Israel) for 24 h to obtain FBS-free conditioned medium. The medium was centrifuged at 4 °C, 6000 g for 6 min to eliminate cells and debris, followed by centrifugation at 4 °C, 12,000 g for 40 min to remove large diameter extracellular vesicles. The supernatant was transferred to new tubes and ultracentrifuged at 4 °C,100,000 g for 70 min in an Optima XPN-100 ultracentrifuge (A94469; Beckman, America) to obtain the exosome precipitate.

The exosome precipitate was suspended in PBS and quantified with bicinchoninic acid (BCA) protein assay kit (P1511-3; Applygen, China) according to the manufacturer's protocol. All the exosomes were used immediately for experiments or stored at − 80 °C for no longer than one week.

The morphology of ADSC-exos and MSGMSC-exos were observed using transmission electron microscopy (JEM-1400, JEOL Corporation, Japan). Nanoparticle tracking analysis (NTA) was performed using ZetaView PMX 110 (Particle Metrix, Germany) to analyze the size distribution of ADSC-exos and MSGMSC-exos. Western blot assay was performed with CD81 (66866-1; Proteintech, America) and TSG101 (14497-1; Proteintech, America) antibodies to analyze the surface markers of exosomes.

Cellular uptake of ADSC-exos and MSGMSC-exos

ADSC-exos and MSGMSC-exos were labeled with PKH26 red fluorescent cell linker (PKH26GL; Merck, America). Human umbilical vein endothelial cells (HUVECs) were seeded in 6-well plates and PKH26-labeled ADSC-exos or MSGMSC-exos were added with an ultimate dose of 20 μg/ml. After 12 h of incubation, HUVECs were fixed with 4% paraformaldehyde and stained with DAPI. Finally, the location of exosomes was confirmed using confocal microscope (Carl Zeiss, Germany).

Cell counting kit-8 (CCK-8) assay

CCK-8 assay (CK04; Dojindo, Japan) was performed to evaluate the effect of ADSC-exos and MSGMSC-exos on the proliferation of HUVECs. HUVECs were initially cultured in DMEM-high glucose (SH30284.01; HyClone, America) with 10% FBS, 100 U/ml penicillin, and 100 μg/ml streptomycin. When reaching 90 percent of confluent, the cells were trypsinized and seeded into four 96-well plates for examination at four different time points at a density of 5×10^3 cells per well. 100 μl FBS-free medium was added to each well for overnight incubation. Subsequently, the medium was changed and the cells were stimulated separately with ADSC-exos, MSGMSC-exos at concentration gradients of 50 μg/ml, 100 μg/ml, and 150 μg/ml, or with FBS-free medium (n = 3). This concentration gradient was established to find the optimal working concentration of ADSC-exos and MSGMSC-exos. At 24, 48, 72, and 96 h, 10 μl of CCK-8 solution was added to each well. The absorbance was measured at 450 nm using a microplate reader (n = 3). The optical density (OD) values were recorded and represented the proliferation of the HUVECs.

Tube formation assay

Tube formation assay was performed to assess the effect of ADSC-exos and MSGMSC-exos on promoting capillary-network formation of HUVECs. 60 μl of Matrigel (356234; BD Bioscience, America) was added to each well of a 96-well plate and incubated in an incubator for gel formation. HUVECs were starved for 24 h using FBS-free medium, then trypsinized and seeded into the 96-well plate precoated with Matrigel at a density of 3×10^4 cells per well. The cells were stimulated with 100 μl FBS-free medium containing 100 μg/ml ADSC-exos, MSGMSC-exos (the concentration was determined based on CCK-8 assay) or an equal volume of FPS-free medium. Tube formation was examined by phase-contrast microscopy at 2, 4, and 8 h. The number of meshes and master junctions was measured by ImageJ software (n = 3).

Cell scratch assay

Cell scratch assay was performed to assess the effect of ADSC-exos and MSGMSC-exos on the migration of HUVECs. HUVECs were seeded into 6-well plates at a density of 1.5×10^5 per well and cultured to reach 100% confluence and form a monolayer. Three parallel scratches were created in each well using a pipette tip. The cells were stimulated with 1 ml FBS-free medium containing 100 μg/ml ADSC-exos, MSGMSC-exos or an equal volume of FPS-free medium. Pictures were taken at 0, 6, 12, 18, 24 h. The migration rate was measured by ImageJ software (n = 3).

Animal model

8-week-old (bodyweight of 25 ± 2 g) male BALB/c mice were purchased from the Experimental Animal Center of Peking University Health Science Center. All animal experiments were approved by the Ethics Committee of Peking University Health Science Center (S2019144). The work has been reported in line with the ARRIVE guidelines 2.0.

The construction of the full-thickness skin defect model strictly adhered to a nature protocol [38]. On the day before surgery, BALB/c mice were anesthetized by intraperitoneal injection of 3 g/L pentobarbital sodium (30 mg/kg) and the fur on the dorsal and lateral skin was removed using an electric hair clipper. Then, the depilatory paste was applied on the formal described area. After 5 min wait, it was wiped out by cotton balls moistened with PBS. The mice were housed individually after finishing epilation to avoid potential skin harm. On the surgery day, the mice were initially anesthetized with pentobarbital sodium, followed by creating two symmetrical 8-mm full-thickness skin defect by a sterile biopsy punch. A ring-shaped silicone splint with 10 mm internal diameters and 18 mm external diameters was fixed by an instant-bonding adhesive and 3–0 thread for each defect. Mice were randomized into four groups. Control group: the wound was covered with 80 μl of PBS (n = 6); GelMa group: the wound was covered with 80 μl of GelMa (SunP Gel G1, SunpBiotech, China) (n = 6); GelMa + ADSC-Exo group: the wound was covered with 80 μl of GelMa combined with ADSC-Exo with an ultimate concentration of 500 μg/ml (n = 6); GelMa + MSGMSC-Exo group: the wound was covered 80 μl of GelMa combined with MSGMSC-Exo with an ultimate concentration of 500 μg/ml (n = 6). The preparation of GelMa hydrogels was described before [39]. Except for the control group, the GelMa in the remaining three groups were irradiated with 380 nm ultraviolet for 15 s to make it light-cured. Finally, Tegaderm (3 M, America) and self-adhering elastic bandage were used to dress the wound. Daily inspection of the mice was carried out to ensure the splint was securely in position. If any tendency to detachment was observed, prompt suturing would be applied. The wound healing was observed and recorded at days 0, 5, 10, and 15 post-operation. The wound healing rate was calculated following this formula: the wound healing rate = {1 – (remaining wound area/primary wound area)} × 100%.

Histological analysis

At 15 days post-operation, all the mice were sacrificed by cervical dislocation. The full thickness skin of the wound area was harvested and immediately observed using a stereo microscope (SMZ800N; Nikon, Japan) to confirm neo-vessel formation. Then it was fixed in 4% paraformaldehyde. The wound skin was subsequently dehydrated, and embedded in paraffin. The paraffin-embedded tissue was cut into 5 μm sections. The sections were stained with hematoxylin and eosin (H&E) and Masson's trichrome to evaluate the overall condition and collagen deposition in the wound beds. The relative collagen expression rate was calculated by ImageJ software (n = 3).

Immunohistochemical (IHC) analysis

To further confirm angiogenesis in the wound beds, immunohistochemical staining for CD31 and α-SMA was performed. Immunohistochemical staining of collagen I and collagen III was performed to determine the effects of ADSC-exos and MSGMSC-exos on scar formation. Immunohistochemical staining for Ki-67 was performed to examine the cells undergoing mitosis, which can evaluate the effects of ADSC-exos and MSGMSC-exos on tissue regeneration. The sections were treated with antigen retrieval and incubated with the following antibody at 4 °C overnight respectively: CD31(1:200, GB113151; Servicebio, China), α-SMA (1:500, BM0002; Bosterbio, China), collagen I (1:500, ab138492; Abcam, England), collagen III (1:500, ab6310; Abcam, England), and

Ki-67(1:1000, ab15580; Abcam, England). Afterwards, the sections were incubated with a secondary antibody at room temperature for 30 min and consequently followed by diaminobenzidine (DAB) and hematoxylin staining, dehydrated, and mounted. Images from 3 samples each group were utilized for quantitative analysis using ImageJ software.

Immunofluorescence staining

To evaluate the effects of MSGMSC-exos and ADSC-exos on anti-inflammation, immunofluorescence staining of F4/80, CD86, CD206, and FOXP3 was performed. Freezed slices were fixed with 4% paraformaldehyde for 10 min, followed by incubated with 0.3% Triton solution for 10 min, then washed with PBS for 3 times. Afterwards, they were blocked in 1% BSA for 1 h at room temperature. The slices were incubated with anti-F4/80 (1:200, ab300421; Abcam, England), CD86 (1:400, 13395-1-AP; Proteintech, America), CD206 (1:200, 81525-1-RR; Proteintech, America) and FOXP3 antibodies (1:200, ab75763; Abcam, England) respectively at 4 °C overnight, followed by incubation with goat anti-rabbit Alexa Fluor® 488 (ab150077; Abcam, England) or Alexa Fluor® 594-conjugated secondary antibody (ab150080; Abcam, England) for 1 h at room temperature. Finally, the samples were stained with DAPI for 10 min and washed with PBS for 3 times. Images from 3 samples each group were used for quantitative analysis utilized ImageJ software.

RNA isolation and quantitative real-time polymerase chain reaction (qPCR)

Total RNA was isolated from HUVECs which were cocultured with 100 μg/ml MSGMSC-exos or 100 μg/ml ADSC-exos for 24 h or harvested mice skin by using TRIzol reagents (15596018CN; Invitrogen, America). cDNA was produced utilizing using a PrimeScript™ RT reagent Kit (RR036B; Takara, Japan). The qPCR was carried out via applying SYBR-Green (G3326; servicebio, China). The primer sequences involved were displayed as follows.

Gene name	Forward (5′–3′)	Reverse (5′–3′)
human-GAPDH	GGAAGCTTGTCATCAATG GAAATC	TGATGACCCTTTTGGCTCCC
human-VEGFA	AGGGCAGAATCATCA CGAAGT	GCACACAGGATGGCTTGA AGA
human-ITGB1	GTTCAGTTTGCTGTGTGT TTGC	ATCCTCTGGCTTGAGCTT CTCT
human-CXCR4	GCCTTATCCTGCCTGGTA TTGT	AGGATGACTGTGGTCTTG AGGG
mouse-GAPDH	CCTCGTCCCGTAGACAAA ATG	TGAGGTCAATGAAGGGGT CGT
mouse-Col1a1	GAGAGGTGAACAAGG TCCCG	AAACCTCTCTCGCCTCTTGC
mouse-MMP1	CCCATCTATACCTACACT GGCAAA	TTTGGGATGCTTAGGGTTGG
mouse-MMP3	GCCAGGATTTCCCAGGAA GATA	AAATTCCAACTGCGAAGA TCCA

Western blot analysis

RIPA buffer (G2002; servicebio, China) was used to extract the total protein of ADSC-exos and MSGMSC-exos. Then the total protein was quantified based on BCA method. The proteins at same concentration were subjected in SDS-PAGE and transferred (PVDF, Millipore, America), followed by the incubation with 5% milk and with the primary antibodies (1:1000, ab134179; Abcam, England) at 4 °C overnight. Overnight incubated membranes were washed by PBST buffer three times, followed by goat anti-rabbit IgG (1:5000, GB23303; Servicebio, China) as secondary antibodies incubated. The grayscale of the images was quantified and calculated using a gel image system (Bio-Rad, America) and the relative level of each band.

Liquid chromatography with tandem mass spectrometry (LC–MS/MS) analysis

Peptides of MSGMSC-exos and ADSC-exos were dissolved with 0.1% formic acid (FA) and the chromatographic separation was performed on a reversed phase C18 column at a flow rate of 300 nL/min with a 60 min gradient of 5 to 40% acetonitrile in 0.1% formic acid. The electrospray voltage was maintained at 2.2 kV and the capillary temperature was set at 300 °C. The MS analysis experiments were performed on a nano-flow high pressure liquid chromatography (HPLC) system (U3000 UHPLC, ThermoFisher Scientific, Waltham, MA, USA) connected to a Q-Exactive HF Mass Spectrometer (ThermoFisher Scientific) equipped with a Nanospray Flex Ion Source (ThermoFisher Scientific). Elisa test was conducted according to the manufacturer's instructions (SEB042Hu, Cloud-Clone Corp, America) to assess the concentrations of the ITGB1 protein.

bioinformation analysis

Raw MS data was processed in maxquant software package (v1.6.6.0). The Uniprot human protein database was used as a reference for protein identification. The identified proteins were compared with ExoCarta database (http://www.exocarta.org). Gene Ontology (GO) and Kyoto Encyclopedia of Genes and Genomes (KEGG) pathway enrichment analysis were performed using the Metascape web service (https://metascape.org/gp/index.html). Protein–protein interaction (PPI) analysis was performed using the STRING web service (https://cn.

string-db.org/cgi/input?sessionId=bjT8qIrGAHWZ). RStudio was used for data visualization.

Statistical analysis

Statistical significance among different groups was determined by one-way analysis of variance (ANOVA) by Tukey's multiple comparisons test in GraphPad Prism 8.0.2. Differences with $P < 0.05$ were considered statistically significant. Data were presented as mean ± standard deviation (SD).

Results

Characterization of ADSCs and MSGMSCs, identification and Cellular uptake of ADSC-exos and MSGMSC-exos

ADSCs and MSGMSCs were extracted and subjected to adipogenic and osteogenic induction. Both stem cell types showed the ability of multiple differentiation potential. Adipocytes, osteoblasts, and chondrocytes could be observed in adipogenic differentiation, osteogenic and chondrogenic induction, respectively (Fig. S1A). Besides, both ADSCs and MSGMSCs were highly positive for mesenchymal stem cell (MSC) surface markers, including CD29, CD105 and CD166, meanwhile negative for hematopoietic stem cell (HSC) surface markers, including CD11b, CD14 and HLA-DR, which indicated both the isolated ADSCs and MSGMSCs were consistent with the typical stem cell characteristics (Fig. S1B). Furthermore, exosomes from ADSCs and MSGMSCs were extracted and observed by transmission electron microscopy (TEM). Exosomes from both ADSCs and MSGMSCs presented sphere-shaped morphology (Fig. S2A) The diameters of ADSC-exos and MSGMSC-exos were approximately 110 nm, measured by NTA analysis (Fig. S2B). Western blot results showed the presence of CD81 and TSG101, namely the marker proteins of exosomes, meanwhile the absence of Calnexin (Fig. S2C). These data indicated that the extraction of ADSC-exos and MSGMSC-exos were successful. The result showed that HUVECs were surrounded with red fluorescence after incubation with ADSC-exos and MSGMSC-exos, indicating that these exosomes could be internalized by HUVECs (Fig. S2D).

MSGMSC-exos and ADSC-exos promote the proliferation of HUVECs similarly in a dose-dependent manner

The proliferation of HUVECs cultured in medium containing different concentrations of MSGMSC-exos or ADSC-exos at 24 h, 48 h, 72 h, and 96 h is shown in Fig. 1. From the results, we can see that ADSC-exos promoted the proliferation of HUVECs at an earlier time point

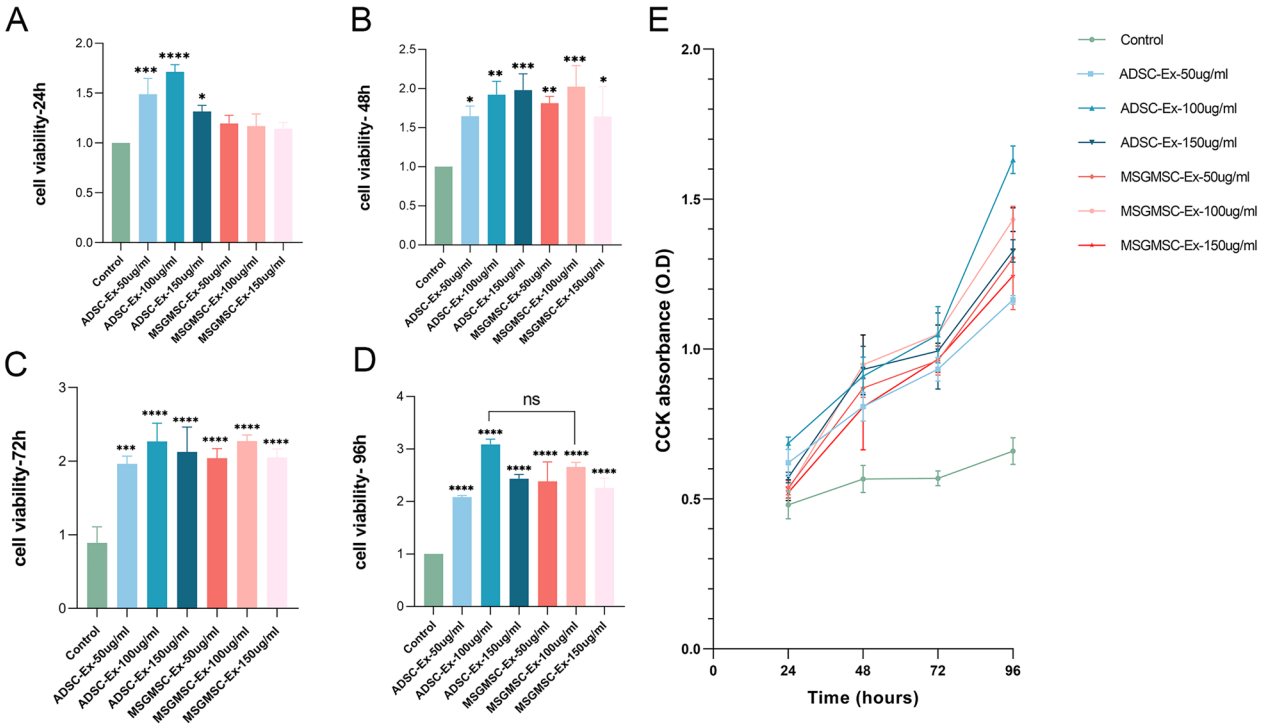

Fig. 1 CCK-8 assay of the effect of ADSC-exos and MSGMSC-exos on HUVECs. (n = 3) **A–D** Cell viability of HUVECs 24 h, 48 h, 72 h, 96 h after treated with ADSC-exos and MSGMSC-exos respectively. **E** The line graph that reveals the O.D value of every group at each time point. *$p < 0.05$, **$p < 0.01$, ***$p < 0.001$, ****$p < 0.0001$

compared to MSGMSC-exos (Fig. 1A). At 24 h, ADSC-exos already significantly promoted the proliferation of HUVECs, whereas MSCMSG-exos did not exhibit the same effect. At 48 h, MSGMSC-exos started to exhibit the effect on promotion HUVECs proliferation similar to that of ADSC-exos (Fig. 1B). At 72 h, almost all groups containing exosomes exerted a proliferative influence on HUVECs very significantly (Fig. 1C). All these groups showed highly significant effect on promoting the proliferation of HUVECs at 96 h. Though the medium containing 100 μg/ml ADSC-exos seemed to perform better than the medium containing 100 μg/ml MSGMSC-exos, the observed difference did not achieve statistical significance (Fig. 1D). The results demonstrated that the optimal working concentration for both ADSC-exos and MSGMSC-exos is 100 μg/ml and both of them work in a dose-dependent manner (Fig. 1A–D). Moreover, the growth rate of HUVECs during this period can be ranked as follows in both ADSC-exos groups and MSGMSC-exos groups: 72–96 h, 24–48 h, 48–72 h, indicating that both ADSC-exos and MSGMSC-exos promote HUVECs proliferation in a similar manner (Fig. 1E).

MSGMSC-exos and ADSC-exos have similar effect on promoting tube formation

After cocultured with 100 μg/ml MSGMSC-exos or 100 μg/ml ADSC-exos for 2 h, the number of meshes and master junctions of MSGMSC-exos group and ADSC-exos group were statistically higher than those in the control group (Fig. 2). Representative images are presented in Fig. 2A. After 4 and 8 h of co-culturing, the distinction between groups containing MSGMSC-exos or ADSC-exos and the control group became increasingly pronounced. Though MSGMSC-exos seemed to perform slightly better than ADSC-exos, there was no statistically significant difference between these two groups (Fig. 2B, C). The number of meshes and master junctions continued to increase throughout the 8-h co-culture duration in both the MSGMSC-exos group and the ADSC-exos group, with a higher growth rate observed during the latter 4 h, while the number of meshes slightly decreased in the control group at 8 h because of partially disintegration of the tubules (Fig. 2D, E).

MSGMSC-exos can promote the migration of HUVECs slightly better than ADSC-exos

Representative images of cell migration results are presented in Fig. 3A. After cocultured with 100 μg/ml MSGMSC-exos or 100 μg/ml ADSC-exos for 12 h, the migration rate of MSGMSC-exos group was statistically higher than control group. Meanwhile, there is no statistically significant difference between ADSC-exos group and control group. After 18 h and 24 h of co-culturing, the migration rates of both the ADSC-exos group and the MSGMSC-exos group are statistically higher than control group (Fig. 3B). The migration rates of each group increased almost uniformly over time, particularly in the control group. At all time points, the MSGMSC-exos group exhibited a slightly superior promotion effect compared to the ADSC-exos group (Fig. 3C). After 24 h of co-culturing, the distinction between MSGMSC-exos group and ADSC-exos group reached statistical significance (Fig. 3B). qPCR was carried out to detect the upregulation of key migration-related gene (VEGFA, ITGB1, and CXCR4). The qPCR results indicated that compared to the Control group, the expression of VEGFA and ITGB1 genes was significantly increased in the MSGMSC-exos and ADSC-exos groups, while the increase in CXCR4 gene expression was not significant (Fig. S3) .

MSGMSC-exos exhibit wound healing efficacy comparable to that of ADSC-exos

Figure 4A illustrates the procedure of in vivo animal study. The gross images of wounds were captured on days 0, 5, 10, and 15 after injury (Fig. 4B). Meanwhile, the wound healing rates were recorded (Fig. 4C). The wound sizes in the MSGMSC-exos group showed more rapid healing than Control and GelMa groups from day 5 post-injury, as confirmed in both gross images and wound healing rates. There was no statistically significant differentiation between the terminal wound healing rate of MSGMSC-exos group and that of ADSC-exos. The promotion of wound healing was initiated by day 5 in the MSGMSC-exos group, whereas this effect was not evident in the ADSC-exos group on the same day.

Figure 5 illustrates representative H&E staining images of different groups by day 15. The area between the two red arrows stands for the wound bed. The wound bed of the MSGMSC-exos and ADSC-exos group showed higher maturity featured by ordered arrangement of fibroblasts and collagenous fiber, continuous basement membrane and reduced infiltration of inflammatory cells comparing to GelMa and control group. By day 15, the MSGMSC-exos group and ADSC-exos group had finished re-epithelialization, while the other two groups showed incomplete re-epithelialization. Appendages such as hair follicles and sebaceous glands failed to regenerate in the wound beds of any of the groups.

Applying MSGMSC-exos or ADSC-exos promotes collagen deposition, cell proliferation and vascularization in the wound bed

Collagen deposition is a crucial component of the wound healing process. Adequate collagen deposition can enhance the tensile strength of the wound, leading to better wound healing. Masson staining revealed

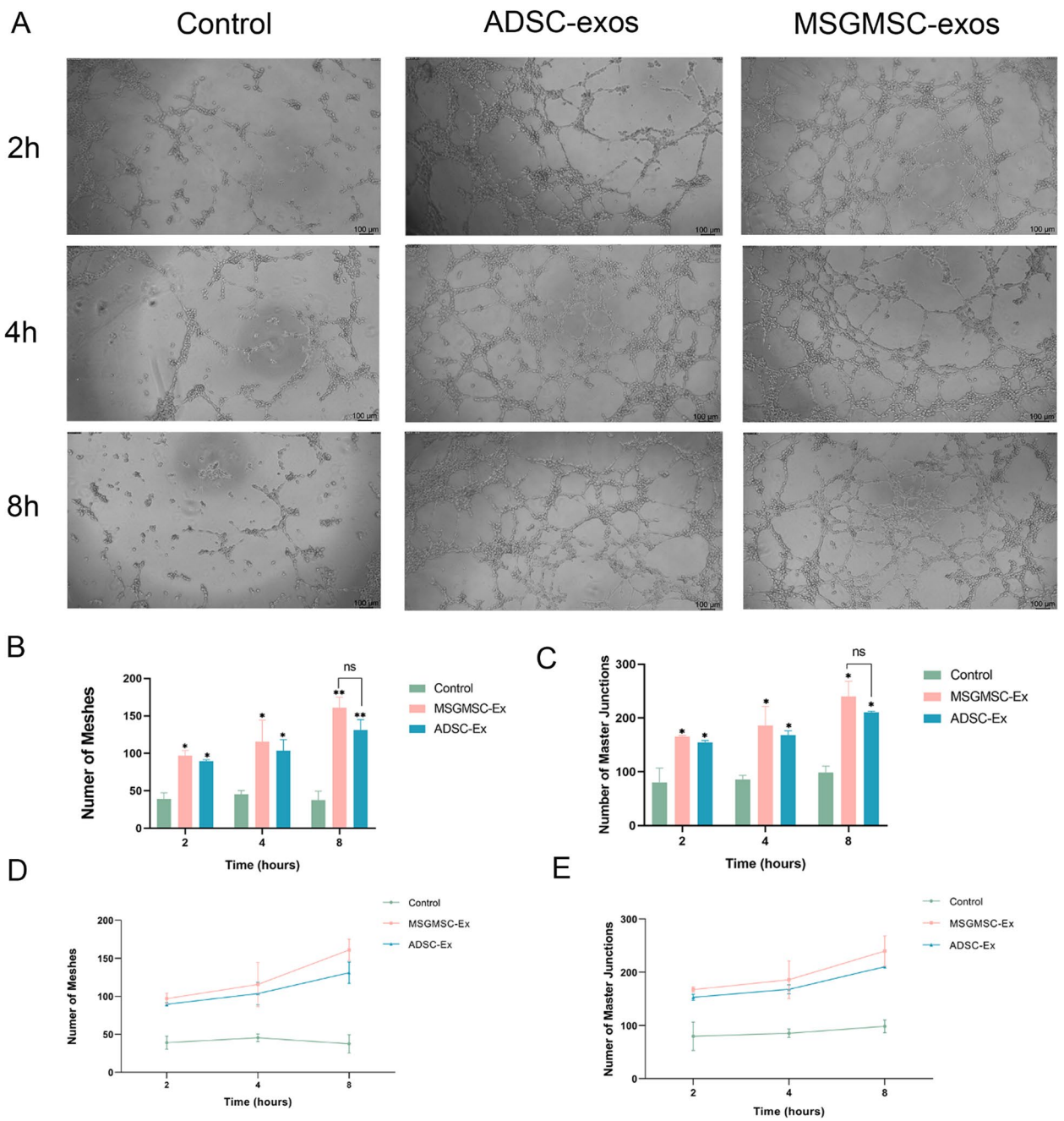

Fig. 2 Results of tube formation assay of HUVECs. (n = 3) **A** Representative images of the formed tubules. (scale bars = 100 μm) **B** The number tube structures per view field of each group. It represents the tubule that has already formed. **C** The number of master junctions per view field of each group. It represents the potential to form new tubules. **D** The line graph of the number of meshes **E** The line graph of the number of master junctions. $^{*}p < 0.05$, $^{**}p < 0.01$

that collagen deposition in both the MSGMSC-exos and ADSC-exos groups was greater than that in the GelMa group, with the ADSC-exos group demonstrating superior collagen deposition compared to the MSGMSC-exos group (Fig. 6A, B). Type III collagen is the predominant collagen type involved in wound healing and constitutes a major component of granulation tissue [40]. Increased collagen III deposition, namely a lower collagen I to collagen III ratio, is essential for minimizing scar [14, 41]. Therefore, we further performed IHC staining for collagen I and collagen III. The results indicated that both ADSC-exos and MSGMSC-exos primarily promoted

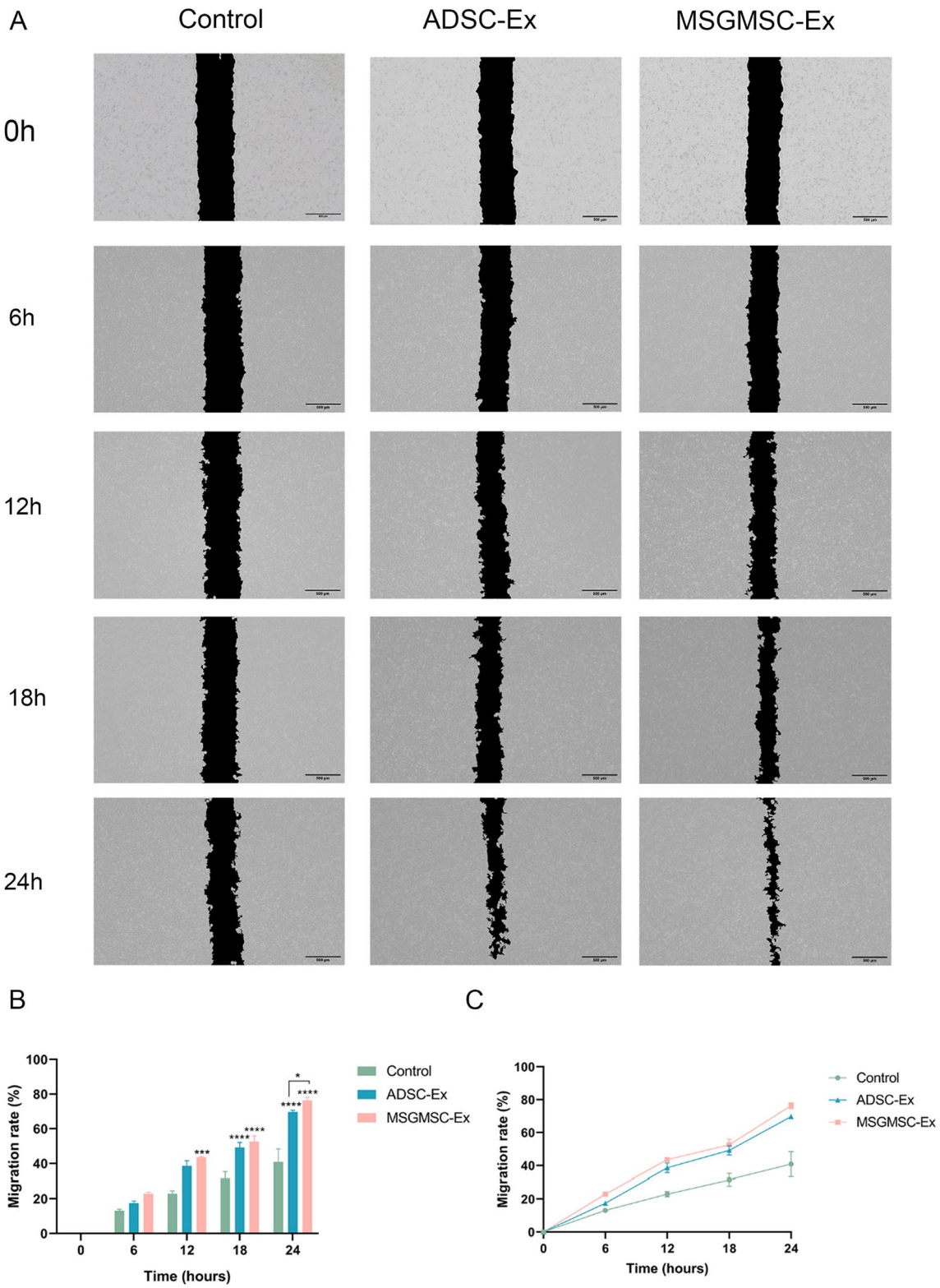

Fig. 3 Cell migration results of HUVECs. (n = 3) **A** Representative images of cell migration results, scale bars = 500 μm. **B** The migration rate of each group over time. *$p < 0.05$, **$p < 0.01$, ***$p < 0.001$, ****$p < 0.0001$. **C** The line graph of the migration rate which can show the growth trend of each group

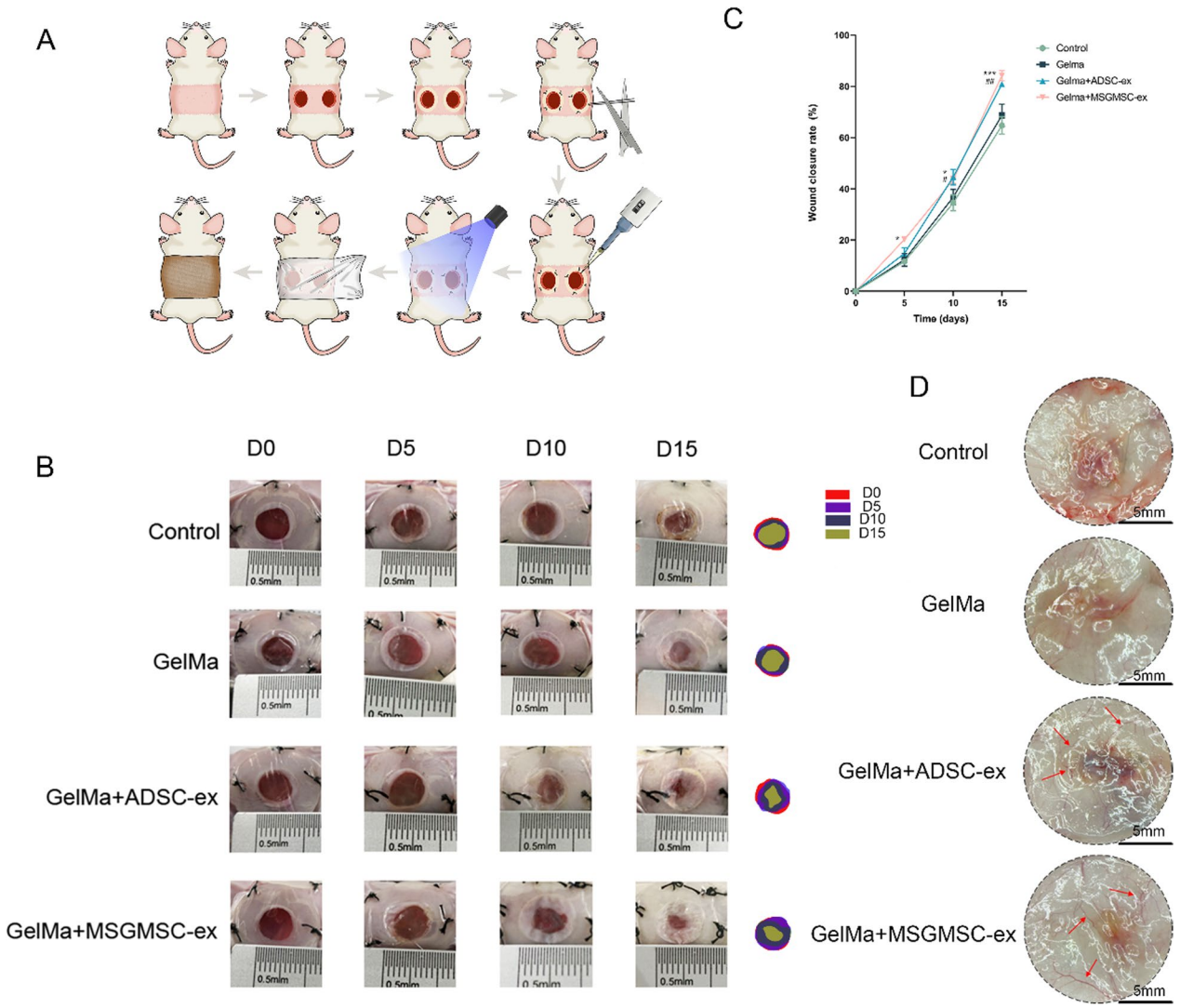

Fig. 4 Healing process of wounds promoted by MSGMSC-exos and ADSC-exos. **A** The procedure of in vivo study. **B** Representative images of wound healing process in Control, GelMa, GelMa + ADSC-exos and GelMa + MSGMSC-exos group. **C** Wound healing rates at different time points of the four groups. (n = 6) $*p < 0.05$, $**p < 0.01$, $***p < 0.001$. $\#p < 0.05$, $\#\#p < 0.01$ (* stands for MSGMSC-exos group vs GelMa group. # stands for ADSC-exos group vs GelMa group). **D** Representative photomicrographs of wounds, showing increased neo-vessel formation (Red arrows) in MSGMSC-exos and ADSC-exos groups (scale bars = 5 mm)

overall collagen deposition by enhancing Type III collagen deposition. The expression of Type I collagen in the MSGMSC-exos group was even lower than that in the GelMa group. The MSGMSC-exos group demonstrated the lowest ratio of collagen I to collagen III, with a statistically significant difference compared to the ADSC-exos group ($P < 0.05$). This suggested that, although the overall collagen deposition in the MSGMSC-exos group was lower than that in the ADSC-exos group, it has a greater potential for preventing scar formation after wound healing. qPCR further confirmed the upregulation of anti-scar genes such as MMP1 and MMP3, and the downregulation of COL1 gene in the MSGMSC-exos group compared to either the ADSC-exos group or the GelMa group (Fig. S4) .

We further conducted IHC staining for Ki67, CD31, and α-SMA to evaluate the proliferation of granulation tissue, angiogenesis and vascular maturation in vivo. The Ki67-positive cells were significantly increased in the MSGMSC-exos and ADSC-exos groups compared to the GelMa and Control groups, indicating that granulation tissue proliferation was improved after exosome treatment (Fig. 7A). CD31 is an endothelial cell marker, commonly expressed in the cells lining the lumen of both

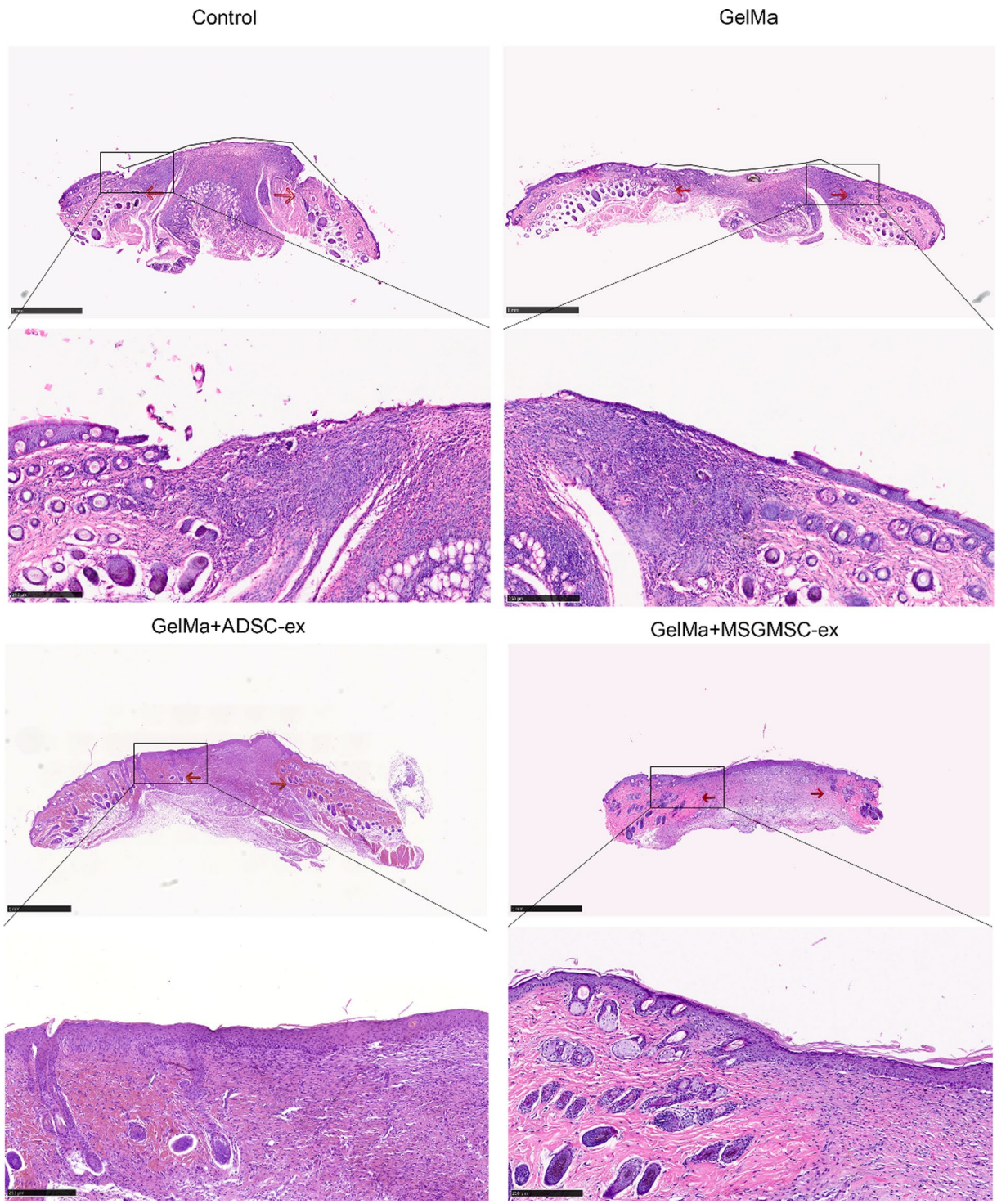

Fig. 5 Representative images of H&E staining in four groups. Red arrows stand for the margin of the wound bed. Black lines stand for the nonepithelialized area in the control and GelMa group (scale bar = 1 mm)

immature and mature blood vessels. The MSGMSC-exos and ADSC-exos groups showed more CD31-positive tubular structures (Fig. 7B), demonstrating that both MSGMSC-exos and ADSC-exos effectively promote angiogenesis in vivo. α-SMA is primarily expressed by vascular smooth muscle cells in the walls of mature blood

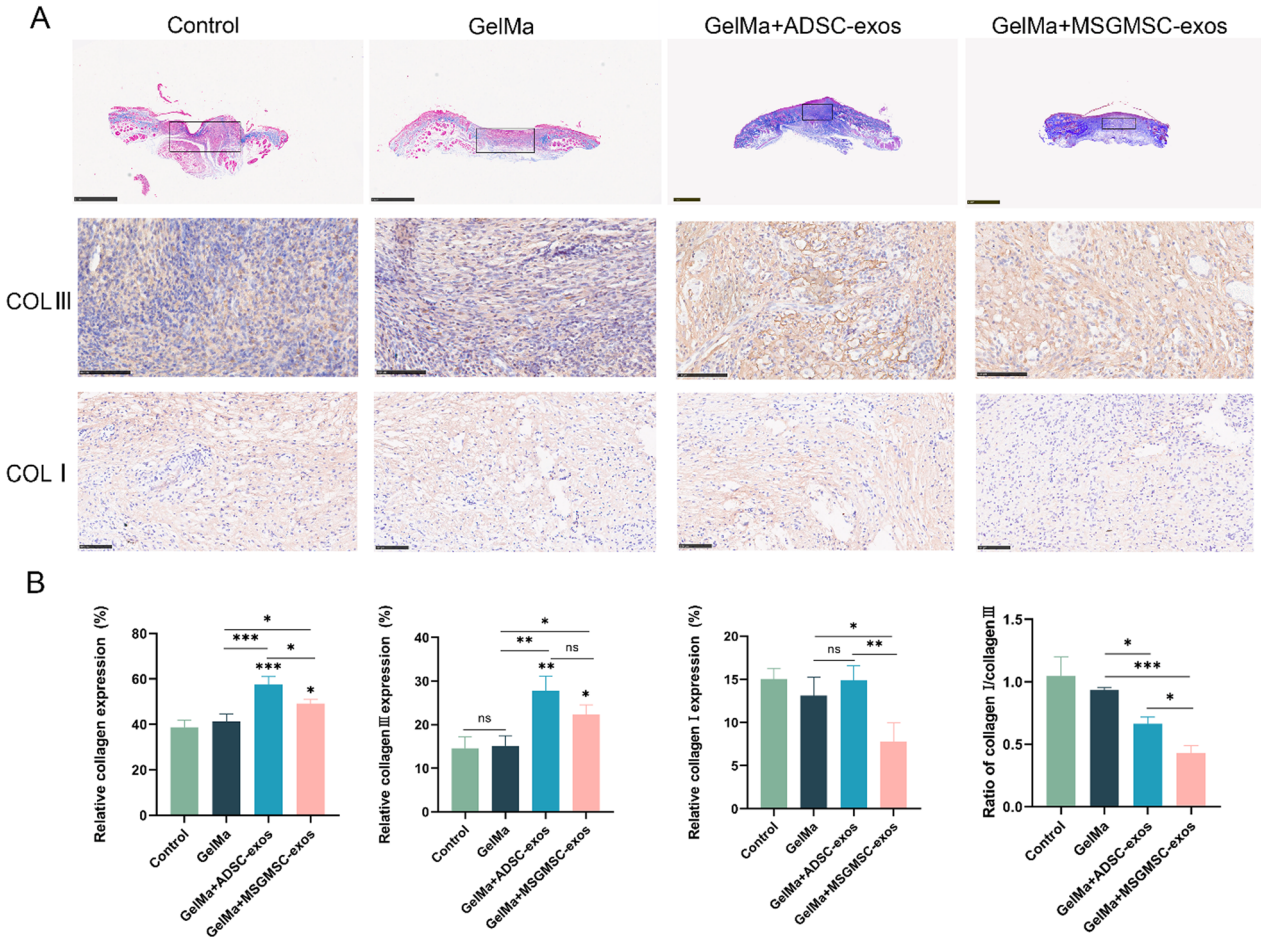

Fig. 6 Collagen deposition of wounds promoted by MSGMSC-exos and ADSC-exos **A** Representative images of Masson staining (scale bars = 1 mm) and immunohistochemical staining of type III collagen and type I collagen (scale bars = 100 μm) in four groups. **B** Quantitative analysis of overall collagen expression, collagen III and collagen I deposition, and collagen I/ collagen III ratio (n = 3). *$p < 0.05$, **$p < 0.01$, ***$p < 0.001$

vessels. Compared to CD31, α-SMA represents more mature blood vessels. α-SMA staining results indicated that both the MSGMSC-exos and ADSC-exos groups exhibited a greater number of mature blood vessels, with no significant statistical difference between these two groups (Fig. 7C).

MSGMSC-exos has a more potent anti-inflammatory effect compared to ADSC-exos

Immunofluorescence staining for F4/80 (pan-macrophage), CD86 (M1 macrophage), CD206 (M2 macrophage), and FOXP3 (regulatory T cells) was conducted to evaluate the inflammation in the wound bed. F4/80-positive cells were slightly reduced in both the MSGMSC-exos and ADSC-exos groups (Fig. 7D, E), with statistical significance only observed in the MSGMSC-exos group ($P < 0.05$). CD86-positive macrophages (the pro-inflammatory M1 phenotype) decreased in both the MSGMSC-exos and ADSC-exos groups, while CD206-positive macrophages (the anti-inflammatory M2 phenotype) increased in both groups. Additionally, the MSGMSC-exos group exhibited a more significant reduction in CD86 expression ($P < 0.05$) and a notable increase in CD206 expression ($P < 0.001$) compared to the ADSC-exos group. This indicates that both MSGMSC-exos and ADSC-exos mediate anti-inflammatory effects by driving M2 polarization of macrophages, with minimal impact on macrophage quantity. Increased M2 macrophage polarization is a hallmark of the transition from the inflammatory phase to the proliferative phase in wound healing [42]. The skin of mice contains a large number of tissue-resident regulatory T cells (Tregs) expressing FOXP3, which can directly suppress inflammation at the wound site through the EGFR pathway, or indirectly by inhibiting the accumulation of pro-inflammatory macrophages, playing a critical role in the regulation of

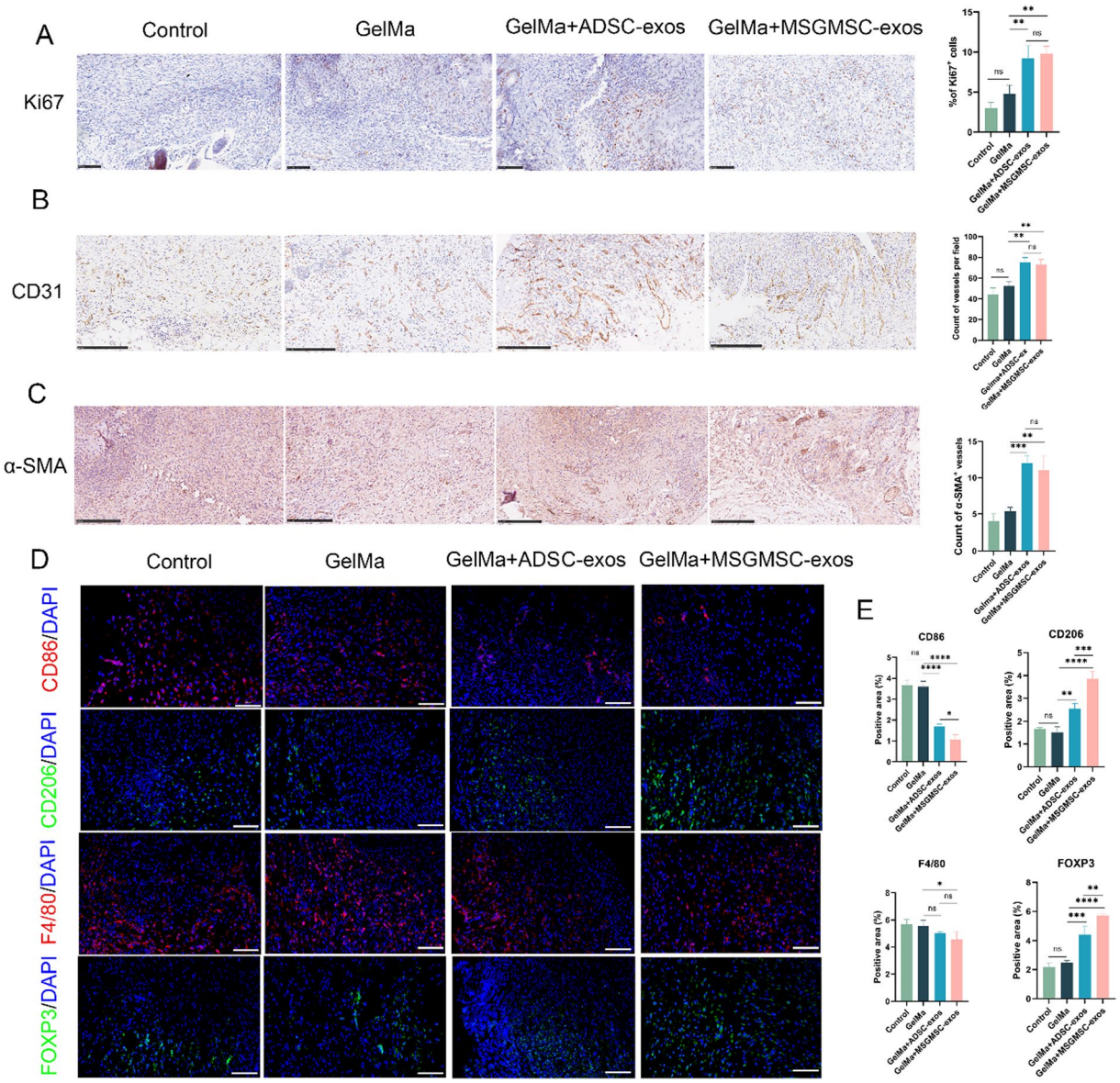

Fig. 7 MSGMSC-exos and ADSC-exos enhance cell proliferation and angiogenesis while suppressing inflammation. **A** Representative images of Ki67 immunohistochemical (scale bars = 100 μm) and quantification of the number of Ki67 positive cells in the wound area (n = 3). **B** Representative images of CD31 immunohistochemical staining (scale bars = 250 μm) and microvessel counts analysis in the wound bed (n = 3). **C** Representative images of α-SMA staining (scale bars = 250 μm) and mature vessels counts analysis (n = 3). **D** Representative images of immunofluorescence staining of macrophages and regulatory T cells in the wound bed (scale bars = 100 μm). **E** Quantitative analysis of the immunofluorescence staining (n = 3). *$p < 0.05$, **$p < 0.01$, ***$p < 0.001$, ****$p < 0.0001$

inflammation at the wound site [43]. Immunofluorescence staining results showed that both MSGMSC-exos and ADSC-exos promoted the accumulation of Tregs, with MSGMSC-exos exhibiting higher FOXP3 expression than ADSC-exos ($P < 0.01$). The above results prove that MSGMSC-exos have a distinct advantage in suppressing wound inflammation compared to ADSC-exos.

Bioinformatics analyses of exosomes from MSGMSC and ADSC

To further explore the mechanism of promoting angiogenesis and wound healing, we conducted proteomic

analysis of exosomes from MSGMSC and ADSC. The result revealed 414 and 408 proteins in MSGMSC-exos and ADSC-exos respectively. 88.16% of the proteins in MSGMSC-exos and 87.5% in ADSC-exos matched those in ExoCarta, indicating that the results were highly reliable. MSGMSC-exos and ADSC-exos had around 83% of proteins in common (Fig. 8A). The Gene Ontology (GO) analysis categorized the results according to biological process (BP), cellular component (CC), and molecular function (MF). In the biological process, proteins in both MSGMSC-exos and ADSC-exos were significantly involved in wound healing, blood coagulation, extracellular matrix organization, and the regulation of angiogenesis (Figs. 8B, 9C). This involvement partly suggests these proteins may facilitate collagen deposition and angiogenesis during the wound healing process. Additionally, other biological processes involved in wound healing, such as tissue migration, epithelial cell migration, and the positive regulation of cell adhesion, were also observed in the GO analysis. In terms of cellular component, proteins in both groups were significantly enriched in extracellular exosome. As for molecular function, proteins in both groups were involved to varying degrees in the structural constituent of the extracellular matrix, collagen binding, and cadherin binding. These molecular functions also play an important role in the wound healing process. Regarding KEGG analysis, both exosome proteins were enriched in Complement and coagulation cascades, ECM-receptor interaction, focal adhesion, and platelet activation (Figs. 8D, 9E).

The volcanogram and heatmap reflected the differences in protein expression between the two groups (Fig. 9A, B). The heatmap indicated that MSGMSC-exos contained more MMP1 and MMP3 proteins which are essential in scarless wound healing. The differential proteins between the two groups are enriched in pathways

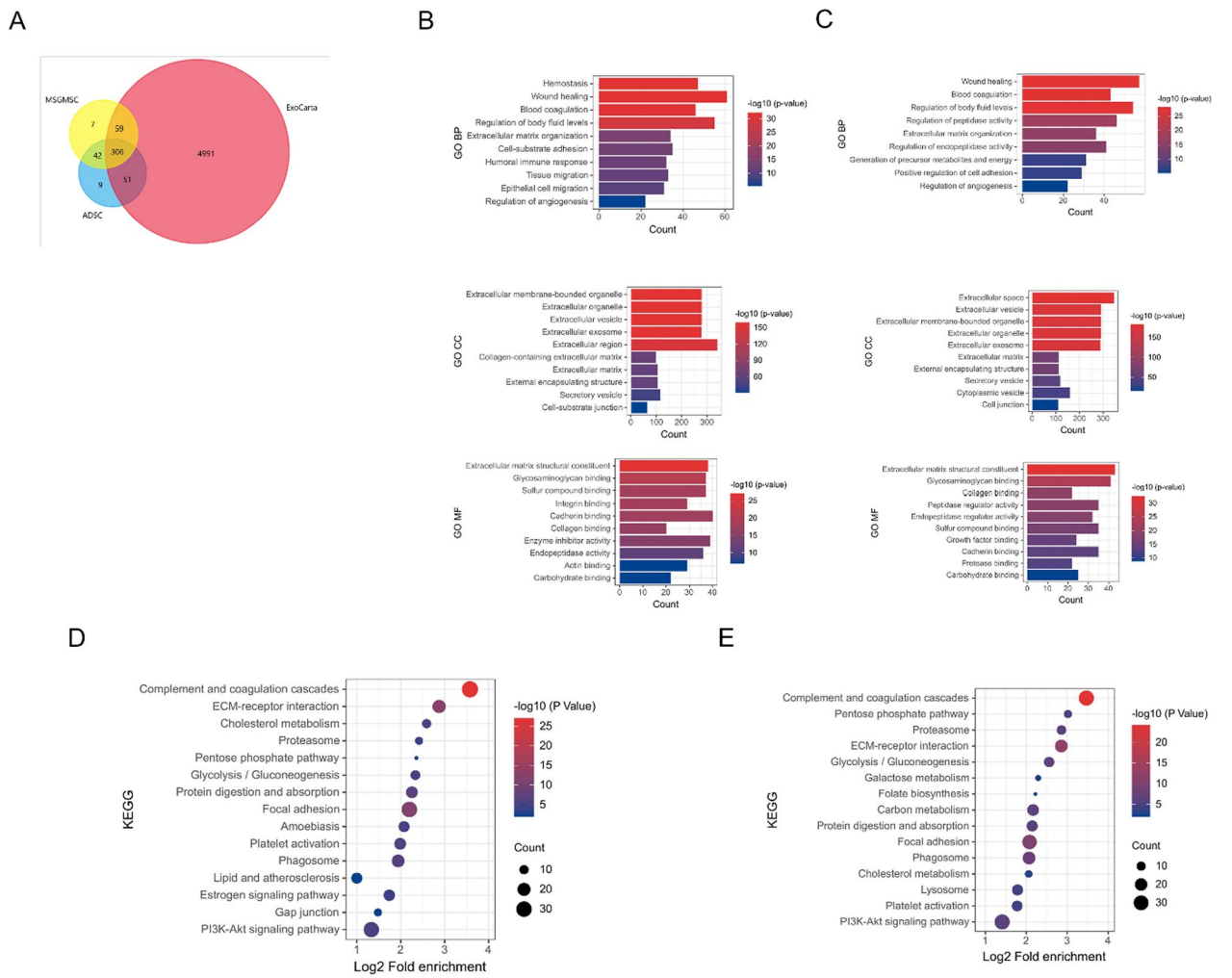

Fig. 8 Bioinformatics analysis of MSGMSC-exos and ADSC-exos. **A** Venn diagram of MSGMSC-exos and ADSC-exos against ExoCarta. **B** GO analysis of ADSC-exos **C** GO analysis of MSGMSC-exos **D** KEGG analysis of ADSC-exos **E** KEGG analysis of MSGMSC-exos

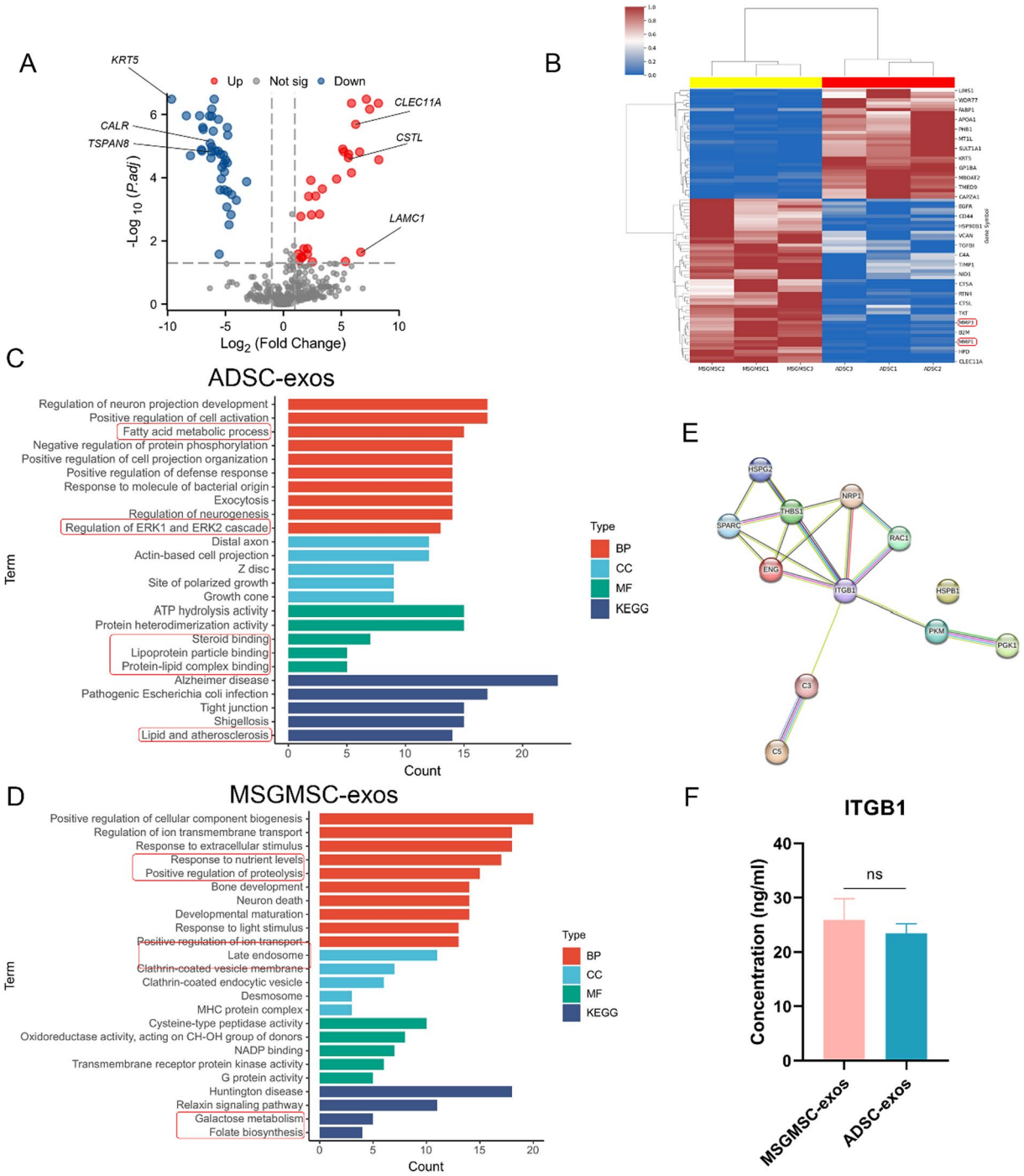

Fig. 9 Bioinformatics analysis of the specific proteins detected in each source of exosomes. **A** The volcanogram of differential proteins for MSGMSC-exos vs ADSC-exos. **B** Heatmap of MSGMSC-exos vs ADSC-exos **C** GO and KEGG analysis of specific proteins for ADSC-exos **D** GO and KEGG analysis of specific proteins for MSGMSC-exos **E** PPI analysis based on shared pro-angiogenic proteins. **F** Elisa test of ITGB1 in MSGMSC-exos and ADSC-exos

such as collagen metabolic process, positive regulation of immune response, and PPAR signaling pathway (Fig. S5), which is consistent with the observed differences in anti-inflammatory and collagen deposition promotion effects in experimental results. Among the differential proteins, those exhibiting highly significant differences

(Log2Fc > 5) and closely associated with wound healing were highlighted in the volcanogram. CLEC11A, CSTL, and LAMC1 were expressed more in MSGMSC-exos, while KRT5, CALR, and TSPAN8 showed higher expression in ADSC-exos. Their specific roles in wound healing are detailed in Supplementary Table 1. Subsequently, we compared the specific BP, CC, MF, and KEGG pathways between the two groups (Fig. 9C, D). ADSC-exos proteins were specifically enriched in fatty acid metabolic process, regulation of ERK1 and ERK2 cascade, lipoprotein particle binding, protein-lipid complex binding and lipid and atherosclerosis. whereas MSGMSC-exos proteins were specifically enriched in response to light stimulus, positive regulation of proteolysis, positive regulation of ion transport, galactose metabolism and folate biosynthesis. These differences may partially reflect the unique characteristics of their source tissues. Proteins in ADSC-exos were more involved in biological processes and diseases related to fat metabolism, while proteins in MSGMSC-exos were highly correlated with certain functions of the salivary gland. 12 pro-angiogenic proteins were identified in both ADSC-exos and MSGMSC-exos, and the details of how they work in promoting angiogenesis can be found in supplementary Table 2. PPI analysis showed that Integrin beta-1 (ITGB1) played a central role among these 12 proteins (Fig. 9E). Results of elisa experiment and western blot confirmed that ITGB1 was present in both ADSC-exos and MSGMSC-exos, and there was no significant difference in concentration between the two groups (Fig. 9F, S6).

Discussion

Exosomes have been extensively studied in the field of promoting wound healing in recent years due to their high safety, easy preservation, low immunogenicity, and fewer ethical issues. Exosomes derived from different mesenchymal stem cells have been proven to have excellent potential in promoting angiogenesis and wound healing. Previous studies have suggested that ADSC-exos have better application prospects because they are easier to obtain and have stable production [44, 45]. However, the complicated process of extracting ADSCs is often underestimated. Extracting ADSCs from liposuction fluid often involves several steps, including PBS washing, enzyme digestion, and centrifugation [46]. Generally, hundreds of milliliters of liposuction fluid need to be processed each time, which is an enormous workload [30]. Despite the long hours of work, the production of each extraction of ADSCs is not satisfactory. Based on our experience, extracting a T75 culture flask of ADSCs requires about 40 ml of pure adipose tissue, or roughly 150 ml of liposuction fluid, which is consistent with previous literature [47]. In contrast, the procedure for extracting MSGMSCs is extremely simple and requires only a minor salivary gland of about 2 X 2 mm to obtain a T75 culture flask of MSGMSCs [34]. Minor salivary glands also have numerous sources: salivary gland biopsy and lip surgery such as cleft palate reconstruction and lipoplasty are all legitimate sources of minor salivary glands [48, 49]. Given these characteristics, MSGMSCs are a promising new source of mesenchymal stem cell exosomes.

Although exosomes from various kinds of mesenchymal stem cells have been proven effective in promoting wound healing, researchers are obsessed with developing new materials to deliver these exosomes, meanwhile ignoring the comparison of the effects and characteristics of different exosomes [50, 51]. This hampers the subsequent selection and development of mesenchymal stem cells and represents a limitation in current research. Currently, only a few studies have evaluated the efficacy differences between different exosomes in promoting wound healing, and their conclusions are controversial. Guo et al. found that ADSC-exos and BMSC-exos have similar effects on wound healing, while Pomatto, M et al. reported that ADSC-exos have better efficacy than BMSC-exos [10, 52]. Although Hoang, D. H et al. did not conduct animal experiments, their results indicate that ADSC-exos, BMSC-exos, and UCSC-exos have similar effects on promoting fibroblast and keratinocyte migration [53]. To accurately assess the efficacy of MSGMSC-exos in promoting wound healing and guide future research directions, we compared them with ADSC-exos in our study. We focused on their effects on promoting angiogenesis since it's a crucial stage during wound healing, and there lacks studies aiming at comparing the angiogenic capabilities of different exosomes.

First, we confirmed the pro-angiogenic capabilities of MSGMSC-exos and ADSC-exos in vitro and in vivo. Both in vitro and in vivo data showed no significant differences in their pro-angiogenic capabilities. Proteomic analysis further demonstrated that both were enriched in regulation of angiogenesis, with ITGB1 playing a central role among the pro-angiogenic proteins. ITGB1 is a membrane-anchoring subunit of many integrins and acts as a mechanosensory protein in endothelial cells [54]. Besides directly interacting with the Vascular Endothelial Growth Factor Receptor (VEGFR), ITGB1 has been identified to promote angiogenesis and regulate endothelial cell adhesion to the extracellular matrix through pathways such as PI3K/AKT and MAPK/ERK [55–58]. The PI3K/AKT and MAPK/ERK signaling pathways are potential candidate targets for ITGB1 protein in promoting wound healing, as their activation has been shown to play a positive role in the wound healing process [59–63]. Besides, more vascular maturation was determined by stereomicroscopy

and α-SMA immunohistochemistry staining, which coincides with ITGB1 is essential in vascular maturation and remodeling [64]. We believe ITGB1 is a potential candidate for enhancing angiogenesis and vascular maturation by MSGMSC-exos and ADSC-exos, similar to the findings of Wu et al [65]. Another interesting finding is that, despite many studies reporting that ADSC-exos upregulate Vascular Endothelial Growth Factor (VEGF) expression in both in vivo and in vitro experiments [66–69]. Proteomic results suggest that neither MSGMSC-exos nor ADSC-exos directly contain VEGFA protein, which is corroborated by several other studies [44, 65, 70, 71]. This implies that the upregulation of VEGF expression by mesenchymal stem cell exosomes may mainly be mediated through their contained microRNAs, such as miR-21 and the let-7 family microRNAs [28, 72].

Combining the in vivo and in vitro experimental results with proteomic sequencing data, we believe that although different types of exosomes are derived from different mesenchymal stem cells, the proteins related to promoting wound healing they contain are relatively conserved. Although previous studies hinted at this, they lacked direct experimental evidence to support it [44, 73–76]. Our experiment provides direct data demonstrating that the effects of MSGMSC-exos and ADSC-exos on promoting wound healing are relatively conserved. MSGMSC-exos are less effective than ADSC-exos in promoting collagen deposition but exhibit superior scar suppression ability. This can be partially attributed to the higher levels of MMP-1 and MMP-3 in MSGMSC-exos, which can prevent excessive collagen deposition, inhibit scar formation, and are associated with scarless healing in fetal tissue by activating the MEK-ERK1/2 MAP kinase signaling pathway and suppressing the TGF-β/Smad pathway [77–79]. The greater anti-inflammatory ability of MSGMSC-exos may be associated with its higher content of CLEC11A protein. Recent studies have validated that CLEC11A is associated with more M2 macrophage polarization and a higher percentage of Treg cells [80]. CLEC11A has been proven to activate the Wnt-β-catenin signaling pathway [81], which is crucial for maintaining the M2 phenotype of macrophages and enhancing the survival of CD4+/CD25+Treg cells [82–84]. Consequently, the Wnt-β-catenin pathway is a primary candidate for the enhanced anti-inflammatory effects of MSGMSC-exos. The primary functional differences in the proteins carried by MSGMSC-exos and ADSC-exos can reflect differences in their tissue sources. The proteins in MSGMSC-exos are specifically enriched in response to light stimulus, positive regulation of ion transport, and folate biosynthesis, which is consistent with findings that light stimuli affect salivary secretion and salivary glands are related to ion transport and folate synthesis [85–88]. In contrast, ADSC-exos are specifically enriched in fatty acid metabolism process, regulation of ERK1/2 cascade, and lipid and atherosclerosis. Evidence also strongly associates these functions with adipose tissue: first, adipose tissue serves as the primary storage site for fatty acids, stored as triglycerides; second, in adipose tissue, the ERK1/2 pathway regulates various functions, including adipocyte differentiation, lipolysis, and insulin sensitivity; and lastly, atheromatous plaques with lipid deposits have been shown to be closely linked to atherosclerosis [89–91].

There are certain limitations to our study. Firstly, while we have identified ITGB1 as a potential candidate for the pro-angiogenic effects of MSGMSC-exos and ADSC-exos, we didn't explore the extent to which blocking ITGB1 would affect angiogenesis, nor the specific mechanisms by which ITGB1 promotes angiogenesis. Secondly, we did not provide mechanistic investigation regarding the differences between MSGMSC-exos and ADSC-exos in collagen deposition and anti-inflammatory effects. Lastly, research has indicated that the pro-inflammatory cytokine IL-17A can enhance the early-stage migration of epithelial cells in wound healing [92]. Given the stronger anti-inflammatory ability exhibited by MSGMSC-exos compared to ADSC-exos, we propose that immediate exosomes application after injuries may not be the most optimal timing, which is worth further investigation. Wound healing is a highly intricate and delicate process, and the aforementioned issues should be further explored in future research.

Conclusions

Our study demonstrates that MSGMSC-exos is a promising novel exosome, showing similar pro-angiogenic and wound healing effects to ADSC-exos, with ITGB1 identified as the core potential pro-angiogenic candidate. Additionally, MSGMSC-exos shows enhanced anti-inflammatory and anti-scar formation effects. Considering the wide availability, easy extraction and culture of MSGMSCs, MSGMSC-exos shows promising application prospects in wound healing treatment.

Abbreviations

MSGMSCs	Minor salivary mesenchymal stem cells
ADSCs	Adipose-derived stem cells
MSGMSC-exos	Exosomes derived from human minor salivary mesenchymal stem cells
ADSC-exos	Exosomes derived from adipose-derived stem cells
HUVECs	Human umbilical vein endothelial cells
BMSCs	Bone marrow-derived stem cells
UCSCs	Umbilical cord derived stem cells
ESCs	Epidermal stem cells
TEM	Transmission electron microscopy
NTA	Nanoparticle tracking analysis
IHC	Immunohistochemical
qPCR	Quantitative real-time polymerase chain reaction
PPI	Protein-protein interaction

Tregs	Regulatory T cells
GO	Gene ontology
KEGG	Kyoto Encyclopedia of Genes and Genomes
ITGB1	Integrin beta-1

Supplementary Information

The online version contains supplementary material available at https://doi.org/10.1186/s13287-024-04069-5.

Supplementary Material 1

Supplementary Material 2

Supplementary Material 3

Supplementary Material 4

Acknowledgements
The authors declare that they have not use AI-generated work in this manuscript.

Author contributions
XH and ZZM designed the study. XH, DP, and QJ performed the experiments. XH, LS, and ZZK analyzed the data. LE and SY evaluated the data. XH wrote and edited the manuscript. LE, SY and SZ revised the work. All authors commented on the manuscript. All authors read and approved the final manuscript.

Funding
This work was supported by the National Natural Science Foundation of China (No. 81871588).

Data availability
The mass spectrometry proteomics data have been deposited in the OMIX, China National Center for Bioinformation with the dataset identifier OMIX007323. Other relevant data are available from the corresponding author upon reasonable request.

Declarations

Ethics approval and consent to participate
The extraction procedures of human MSGMSCs and ADSCs were conducted in accordance with the Declaration of Helsinki, and informed consent was obtained from the donors and/or their guardians before the tooth collection. The animal experiments were conducted following the ARRIVE guidelines 2.0 (Animal Research: Reporting of In Vivo Experiments). The extraction procedures of human MSGMSCs and all animal experiments in this study were approved by the Ethics Committee of Peking University Third Hospital (Project title: Research on the tissue engineering and regenerative medicine application of human minor salivary mesenchymal stem cells No: S2019144, Date of approval: December 19, 2019). The extraction procedures of human ADSCs in this study was approved by the Ethics Committee of Peking University Third Hospital (Project title: Basic research of the application of adipose tissue in the field of plastic surgery No: LM2020365, Date of approval: October 21, 2020).

Consent for publication
Not applicable.

Competing interests
The authors declare that they have no competing interests.

Author details
[1]Department of Plastic Surgery, Peking University Third Hospital, No. 49 North Garden Road, Haidian District, Beijing 100191, China. [2]Department of Plastic and Reconstructive Surgery, Seoul National University College of Medicine, 101 Daehak-ro, Jongno-gu, Seoul 03080, Republic of Korea.

Received: 17 September 2024 Accepted: 20 November 2024
Published online: 03 December 2024

References

1. Butler CE, Orgill DP. Simultaneous in vivo regeneration of neodermis, epidermis, and basement membrane. Adv Biochem Eng Biotechnol. 2005;94:23–41. https://doi.org/10.1007/b99998.
2. Singer AJ, Clark RA. Cutaneous wound healing. N Engl J Med. 1999;341(10):738–46. https://doi.org/10.1056/nejm199909023411006.
3. Zhao P, Sui BD, Liu N, et al. Anti-aging pharmacology in cutaneous wound healing: effects of metformin, resveratrol, and rapamycin by local application. Aging Cell. 2017;16(5):1083–93. https://doi.org/10.1111/acel.12635.
4. Simman R. Wound closure and the reconstructive ladder in plastic surgery. J Am Coll Certified Wound Special. 2009;1(1):6–11. https://doi.org/10.1016/j.jcws.2008.10.003.
5. Boyce DE, Shokrollahi K. Reconstructive surgery. BMJ (Clin Res Ed). 2006;332(7543):710–2. https://doi.org/10.1136/bmj.332.7543.710.
6. Pop MA, Almquist BD. Biomaterials: a potential pathway to healing chronic wounds? Exp Dermatol. 2017;26(9):760–3. https://doi.org/10.1111/exd.13290.
7. Marofi F, Alexandrovna KI, Margiana R, et al. MSCs and their exosomes: a rapidly evolving approach in the context of cutaneous wounds therapy. Stem Cell Res Ther. 2021;12(1):597. https://doi.org/10.1186/s13287-021-02662-6.
8. Kolimi P, Narala S, Nyavanandi D, Youssef AAA, Dudhipala N. Innovative treatment strategies to accelerate wound healing: trajectory and recent advancements. Cells. 2022. https://doi.org/10.3390/cells11152439.
9. Ding J, Wang X, Chen B, Zhang J, Xu J. Exosomes derived from human bone marrow mesenchymal stem cells stimulated by deferoxamine accelerate cutaneous wound healing by promoting angiogenesis. Biomed Res Int. 2019;2019:9742765. https://doi.org/10.1155/2019/9742765.
10. Guo J, Hu H, Gorecka J, et al. Adipose-derived mesenchymal stem cells accelerate diabetic wound healing in a similar fashion as bone marrow-derived cells. Am J Physiol Cell Physiol. 2018;315(6):C885-c896. https://doi.org/10.1152/ajpcell.00120.2018.
11. Wang P, Theocharidis G, Vlachos IS, et al. Exosomes derived from epidermal stem cells improve diabetic wound healing. J Invest Dermatol. 2022;142(9):2508-2517.e13. https://doi.org/10.1016/j.jid.2022.01.030.
12. Hassanshahi A, Hassanshahi M, Khabbazi S, et al. Adipose-derived stem cells for wound healing. J Cell Physiol. 2019;234(6):7903–14. https://doi.org/10.1002/jcp.27922.
13. He L, Zhu C, Jia J, et al. ADSC-Exos containing MALAT1 promotes wound healing by targeting miR-124 through activating Wnt/β-catenin pathway. 2020. Biosci Rep. https://doi.org/10.1042/bsr20192549.
14. Long C, Wang J, Gan W, Qin X, Yang R, Chen X. Therapeutic potential of exosomes from adipose-derived stem cells in chronic wound healing. Front Surg. 2022;9:1030288. https://doi.org/10.3389/fsurg.2022.1030288.
15. Qin X, He J, Wang X, Wang J, Yang R, Chen X. The functions and clinical application potential of exosomes derived from mesenchymal stem cells on wound repair: a review of recent research advances. Front Immunol. 2023;14:1256687. https://doi.org/10.3389/fimmu.2023.1256687.
16. Hu L, Wang J, Zhou X, et al. Exosomes derived from human adipose mensenchymal stem cells accelerates cutaneous wound healing via optimizing the characteristics of fibroblasts. Sci Rep. 2016;6(1):32993. https://doi.org/10.1038/srep32993.
17. Lv H, Liu H, Sun T, Wang H, Zhang X, Xu W. Exosome derived from stem cell: A promising therapeutics for wound healing. Front Pharmacol. 2022;13: 957771. https://doi.org/10.3389/fphar.2022.957771.
18. An Y, Lin S, Tan X, et al. Exosomes from adipose-derived stem cells and application to skin wound healing. Cell Prolif. 2021;54(3):e12993. https://doi.org/10.1111/cpr.12993.
19. Thittamaranahalli Muguregowda H, Pramod K, Echalasara Govindarama Padmanabha U, Sudesh K, Udaya K, Pragna R. Role of angiogenesis and angiogenic factors in acute and chronic wound healing. Plastic Aesthetic Res. 2015;2:243–9. https://doi.org/10.4103/2347-9264.165438.
20. Johnson KE, Wilgus TA. Vascular endothelial growth factor and angiogenesis in the regulation of cutaneous wound repair. Adv Wound Care. 2014;3(10):647–61. https://doi.org/10.1089/wound.2013.0517.
21. DiPietro LA. Angiogenesis and wound repair: when enough is enough. J Leukoc Biol. 2016;100(5):979–84. https://doi.org/10.1189/jlb.4MR0316-102R.

22. Veith AP, Henderson K, Spencer A, Sligar AD, Baker AB. Therapeutic strategies for enhancing angiogenesis in wound healing. Adv Drug Deliv Rev. 2019;146:97–125. https://doi.org/10.1016/j.addr.2018.09.010.
23. Zhao L, Johnson T, Liu D. Therapeutic angiogenesis of adipose-derived stem cells for ischemic diseases. Stem Cell Res Ther. 2017;8(1):125. https://doi.org/10.1186/s13287-017-0578-2.
24. Yang WZ, Yang J, Xue LP, Xiao LB, Li Y. MiR-126 overexpression inhibits high glucose-induced migration and tube formation of rhesus macaque choroid-retinal endothelial cells by obstructing VEGFA and PIK3R2. J Diabetes Comp. 2017;31(4):653–63. https://doi.org/10.1016/j.jdiacomp.2016.12.004.
25. Zhu LL, Huang X, Yu W, Chen H, Chen Y, Dai YT. Transplantation of adipose tissue-derived stem cell-derived exosomes ameliorates erectile function in diabetic rats. Andrologia. 2018;50(2):e12871. https://doi.org/10.1111/and.12871.
26. Liang X, Zhang L, Wang S, Han Q, Zhao RC. Exosomes secreted by mesenchymal stem cells promote endothelial cell angiogenesis by transferring miR-125a. J Cell Sci. 2016;129(11):2182–9. https://doi.org/10.1242/jcs.170373.
27. Kang T, Jones TM, Naddell C, et al. Adipose-derived stem cells induce angiogenesis via microvesicle transport of miRNA-31. Stem Cells Transl Med. 2016;5(4):440–50. https://doi.org/10.5966/sctm.2015-0177.
28. An Y, Zhao J, Nie F, et al. Exosomes from adipose-derived stem cells (ADSCs) overexpressing miR-21 promote vascularization of endothelial cells. Sci Rep. 2019;9(1):12861. https://doi.org/10.1038/s41598-019-49339-y.
29. Dixit VV, Wagh MS. Unfavourable outcomes of liposuction and their management. Indian J Plast Surg. 2013;46(2):377–92. https://doi.org/10.4103/0970-0358.118617.
30. Francis MP, Sachs PC, Elmore LW, Holt SE. Isolating adipose-derived mesenchymal stem cells from lipoaspirate blood and saline fraction. Organogenesis. 2010;6(1):11–4. https://doi.org/10.4161/org.6.1.10019.
31. Glim JE, van Egmond M, Niessen FB, Everts V, Beelen RH. Detrimental dermal wound healing: what can we learn from the oral mucosa? Wound Repair Regen. 2013;21(5):648–60. https://doi.org/10.1111/wrr.12072.
32. Mohanty T, Alberius P, Schmidtchen A, Reiss K, Schröder JM, Sørensen OE. Saliva induces expression of antimicrobial peptides and promotes intracellular killing of bacteria in keratinocytes by epidermal growth factor receptor transactivation. Br J Dermatol. 2017;176(2):403–12. https://doi.org/10.1111/bjd.14883.
33. Kessler AT, Bhatt AA. Review of the major and minor salivary glands, part 1: anatomy, infectious, and inflammatory processes. J Clin Imaging Sci. 2018;8:47. https://doi.org/10.4103/jcis.JCIS_45_18.
34. Lu L, Li Y, Du MJ, et al. Characterization of a self-renewing and multipotent cell population isolated from human minor salivary glands. Sci Rep. 2015;5:10106. https://doi.org/10.1038/srep10106.
35. Pu W, Xu D, Zhang C, Zhao Z, Yang M. Rapid generation of functional hepatocyte-like cells from human minor salivary gland-derived stem cells. Biochem Biophys Res Commun. 2020;522(3):805–10. https://doi.org/10.1016/j.bbrc.2019.11.173.
36. Zhang C, Li Y, Zhang XY, et al. Therapeutic potential of human minor salivary gland epithelial progenitor cells in liver regeneration. Sci Rep. 2017;7(1):12707. https://doi.org/10.1038/s41598-017-11880-z.
37. Nie F, Ding P, Zhang C, Zhao Z, Bi H. Extracellular vesicles derived from lipoaspirate fluid promote fat graft survival. Adipocyte. 2021;10(1):293–309. https://doi.org/10.1080/21623945.2021.1932355.
38. Wang X, Ge J, Tredget EE, Wu Y. The mouse excisional wound splinting model, including applications for stem cell transplantation. Nat Protoc. 2013;8(2):302–9. https://doi.org/10.1038/nprot.2013.002.
39. Zhang X, Ding P, Chen Y, Lin Z, Zhao X, Xie H. Human umbilical cord mesenchymal stem cell-derived exosomes combined with gelatin methacryloyl hydrogel to promote fractional laser injury wound healing. Int Wound J. 2023. https://doi.org/10.1111/iwj.14295.
40. Tejiram S, Zhang J, Travis TE, et al. Compression therapy affects collagen type balance in hypertrophic scar. J Surg Res. 2016;201(2):299–305. https://doi.org/10.1016/j.jss.2015.10.040.
41. Volk SW, Wang Y, Mauldin EA, Liechty KW, Adams SL. Diminished type III collagen promotes myofibroblast differentiation and increases scar deposition in cutaneous wound healing. Cells Tissues Organs. 2011;194(1):25–37. https://doi.org/10.1159/000322399.
42. Whitaker R, Hernaez-Estrada B, Hernandez RM, Santos-Vizcaino E, Spiller KL. Immunomodulatory biomaterials for tissue repair. Chem Rev. 2021;121(18):11305–35. https://doi.org/10.1021/acs.chemrev.0c00895.
43. Nosbaum A, Prevel N, Truong HA, et al. Cutting edge: regulatory T cells facilitate cutaneous wound healing. J Immunol (Baltimore, Md: 1950). 2016;196(5):2010–4. https://doi.org/10.4049/jimmunol.1502139.
44. Wang ZG, He ZY, Liang S, Yang Q, Cheng P, Chen AM. Comprehensive proteomic analysis of exosomes derived from human bone marrow, adipose tissue, and umbilical cord mesenchymal stem cells. Stem Cell Res Ther. 2020;11(1):511. https://doi.org/10.1186/s13287-020-02032-8.
45. Lee JH, Ha DH, Go HK, et al. Reproducible large-scale isolation of exosomes from adipose tissue-derived mesenchymal stem/stromal cells and their application in acute kidney injury. Int J Mol Sci. 2020. https://doi.org/10.3390/ijms21134774.
46. Haack-Sørensen M, Follin B, Juhl M, et al. Culture expansion of adipose derived stromal cells. A closed automated quantum cell expansion system compared with manual flask-based culture. J Transl Med. 2016;14(1):319. https://doi.org/10.1186/s12967-016-1080-9.
47. Schmitz D, Robering JW, Weisbach V, et al. Specific features of ex-obese patients significantly influence the functional cell properties of adipose-derived stromal cells. J Cell Mol Med. 2022;26(16):4463–78. https://doi.org/10.1111/jcmm.17471.
48. Pellegrini M, Pulicari F, Zampetti P, Scribante A, Spadari F. Current salivary glands biopsy techniques: a comprehensive review. Healthcare (Basel, Switzerland). 2022. https://doi.org/10.3390/healthcare10081537.
49. Liao R, Yang HT, Li H, et al. Recent advances of salivary gland biopsy in Sjögren's syndrome. Front Med. 2021;8: 792593. https://doi.org/10.3389/fmed.2021.792593.
50. Geng X, Qi Y, Liu X, Shi Y, Li H, Zhao L. A multifunctional antibacterial and self-healing hydrogel laden with bone marrow mesenchymal stem cell-derived exosomes for accelerating diabetic wound healing. Biomater Adv. 2022;133: 112613. https://doi.org/10.1016/j.msec.2021.112613.
51. Zhou Y, Zhang XL, Lu ST, et al. Human adipose-derived mesenchymal stem cells-derived exosomes encapsulated in pluronic F127 hydrogel promote wound healing and regeneration. Stem Cell Res Ther. 2022;13(1):407. https://doi.org/10.1186/s13287-022-02980-3.
52. Pomatto M, Gai C, Negro F, et al. Differential therapeutic effect of extracellular vesicles derived by bone marrow and adipose mesenchymal stem cells on wound healing of diabetic ulcers and correlation to their cargoes. Int J Mol Sci. 2021. https://doi.org/10.3390/ijms22083851.
53. Hoang DH, Nguyen TD, Nguyen HP, et al. Differential wound healing capacity of mesenchymal stem cell-derived exosomes originated from bone marrow, adipose tissue and umbilical cord under serum- and Xeno-free condition. Front Mol Biosci. 2020;7:119. https://doi.org/10.3389/fmolb.2020.00119.
54. Lorenz L, Axnick J, Buschmann T, et al. Mechanosensing by β1 integrin induces angiocrine signals for liver growth and survival. Nature. 2018;562(7725):128–32. https://doi.org/10.1038/s41586-018-0522-3.
55. Lu Q, Xie Z, Yan C, et al. SNRK (sucrose nonfermenting 1-related kinase) promotes angiogenesis in vivo. Arterioscler Thromb Vasc Biol. 2018;38(2):373–85. https://doi.org/10.1161/atvbaha.117.309834.
56. Pang X, He X, Qiu Z, et al. Targeting integrin pathways: mechanisms and advances in therapy. Signal Transduction Target Ther. 2023;8(1):1. https://doi.org/10.1038/s41392-022-01259-6.
57. Su C, Mo J, Dong S, Liao Z, Zhang B, Zhu P. Integrinβ-1 in disorders and cancers: molecular mechanisms and therapeutic targets. Cell Commun Signal. 2024;22(1):71. https://doi.org/10.1186/s12964-023-01338-3.
58. Yang X, Wang S, Yu W, Zheng Y, Wu Y. Inhibition of ITGB1 enhance the anti-tumor effect of cetuximab in colorectal cancer cell. Medicine. 2020;99(27):e20944. https://doi.org/10.1097/md.0000000000020944.
59. Guo J, Hu Z, Yan F, et al. Angelica dahurica promoted angiogenesis and accelerated wound healing in db/db mice via the HIF-1α/PDGF-β signaling pathway. Free Radic Biol Med. 2020;160:447–57. https://doi.org/10.1016/j.freeradbiomed.2020.08.015.
60. Yuan X, Han L, Fu P, et al. Cinnamaldehyde accelerates wound healing by promoting angiogenesis via up-regulation of PI3K and MAPK signaling pathways. Lab Investig. 2018;98(6):783–98. https://doi.org/10.1038/s41374-018-0025-8.
61. Qu K, Cha H, Ru Y, Que H, Xing M. Buxuhuayu decoction accelerates angiogenesis by activating the PI3K-Akt-eNOS signalling pathway in

a streptozotocin-induced diabetic ulcer rat model. J Ethnopharmacol. 2021;273:113824. https://doi.org/10.1016/j.jep.2021.113824.
62. Balli M, Vitali F, Janiszewski A, et al. Autologous micrograft accelerates endogenous wound healing response through ERK-induced cell migration. Cell Death Differ. 2020;27(5):1520–38. https://doi.org/10.1038/s41418-019-0433-3.
63. Phimnuan P, Dirand Z, Tissot M, et al. Beneficial effects of a blended fibroin/aloe gel extract film on the biomolecular mechanism(s) via the MAPK/ERK pathway relating to diabetic wound healing. ACS Omega. 2023;8(7):6813–24. https://doi.org/10.1021/acsomega.2c07507.
64. Turlo KA, Scapa J, Bagher P, et al. β1-integrin is essential for vasoregulation and smooth muscle survival in vivo. Arterioscler Thromb Vasc Biol. 2013;33(10):2325–35. https://doi.org/10.1161/atvbaha.112.300648.
65. Wu SC, Kuo PJ, Rau CS, et al. Increased angiogenesis by exosomes secreted by adipose-derived stem cells upon lipopolysaccharide stimulation. Int J Mol Sci. 2021. https://doi.org/10.3390/ijms22168877.
66. Ren S, Chen J, Duscher D, et al. Microvesicles from human adipose stem cells promote wound healing by optimizing cellular functions via AKT and ERK signaling pathways. Stem Cell Res Ther. 2019;10(1):47. https://doi.org/10.1186/s13287-019-1152-x.
67. Zhang X, Jiang Y, Huang Q, et al. Exosomes derived from adipose-derived stem cells overexpressing glyoxalase-1 protect endothelial cells and enhance angiogenesis in type 2 diabetic mice with limb ischemia. Stem Cell Res Ther. 2021;12(1):403. https://doi.org/10.1186/s13287-021-02475-7.
68. Han Y, Ren J, Bai Y, Pei X, Han Y. Exosomes from hypoxia-treated human adipose-derived mesenchymal stem cells enhance angiogenesis through VEGF/VEGF-R. Int J Biochem Cell Biol. 2019;109:59–68. https://doi.org/10.1016/j.biocel.2019.01.017.
69. Sun Y, Ju Y, Fang B. Exosomes from human adipose-derived mesenchymal stromal/stem cells accelerate angiogenesis in wound healing: implication of the EGR-1/lncRNA-SENCR/DKC1/VEGF-A axis. Hum Cell. 2022;35(5):1375–90. https://doi.org/10.1007/s13577-022-00732-2.
70. Xing X, Han S, Cheng G, Ni Y, Li Z, Li Z. Proteomic analysis of exosomes from adipose-derived mesenchymal stem cells: a novel therapeutic strategy for tissue injury. Biomed Res Int. 2020;2020:6094562. https://doi.org/10.1155/2020/6094562.
71. Huang LH, Rau CS, Wu SC, et al. Identification and characterization of hADSC-derived exosome proteins from different isolation methods. J Cell Mol Med. 2021;25(15):7436–50. https://doi.org/10.1111/jcmm.16775.
72. Zhu Y, Zhang J, Hu X, Wang Z, Wu S, Yi Y. Extracellular vesicles derived from human adipose-derived stem cells promote the exogenous angiogenesis of fat grafts via the let-7/AGO1/VEGF signalling pathway. Sci Rep. 2020;10(1):5313. https://doi.org/10.1038/s41598-020-62140-6.
73. Ragni E, Banfi F, Barilani M, et al. Extracellular vesicle-shuttled mRNA in mesenchymal stem cell communication. Stem cells (Dayton, Ohio). 2017;35(4):1093–105. https://doi.org/10.1002/stem.2557.
74. Liu B, Qiao G, Cao W, et al. Proteomics analyses reveal functional differences between exosomes of mesenchymal stem cells derived from the umbilical cord and those derived from the adipose tissue. Cell J. 2021;23(1):75–84. https://doi.org/10.22074/cellj.2021.6969.
75. Shin S, Lee J, Kwon Y, et al. Comparative proteomic analysis of the mesenchymal stem cells secretome from adipose, bone marrow, placenta and Wharton's Jelly. Int J Mol Sci. 2021. https://doi.org/10.3390/ijms22020845.
76. Xu X, Yin F, Guo M, et al. Quantitative proteomic analysis of exosomes from umbilical cord mesenchymal stem cells and rat bone marrow stem cells. Proteomics. 2023;23(1): e2200204. https://doi.org/10.1002/pmic.202200204.
77. Li Y, Kilani RT, Rahmani-Neishaboor E, Jalili RB, Ghahary A. Kynurenine increases matrix metalloproteinase-1 and -3 expression in cultured dermal fibroblasts and improves scarring in vivo. J Investig Dermatol. 2014;134(3):643–50. https://doi.org/10.1038/jid.2013.303.
78. Zhang T, Wang X-F, Wang Z-C, et al. Current potential therapeutic strategies targeting the TGF-β/Smad signaling pathway to attenuate keloid and hypertrophic scar formation. Biomed Pharmacother. 2020;129:110287. https://doi.org/10.1016/j.biopha.2020.110287.
79. Peled ZM, Phelps ED, Updike DL, et al. Matrix metalloproteinases and the ontogeny of scarless repair: the other side of the wound healing balance. Plast Reconstr Surg. 2002;110(3):801–11. https://doi.org/10.1097/00006534-200209010-00013.
80. Zheng Q, Gong Z, Li B, et al. Identification and characterization of CLEC11A and its derived immune signature in gastric cancer. Front Immunol. 2024;15:1324959. https://doi.org/10.3389/fimmu.2024.1324959.
81. Xu K, Huang RQ, Wen R, Yang Y, Cheng Y, Chang B. The role of Clec11a in bone construction and remodeling. Front Endocrinol. 2024;15:1429567. https://doi.org/10.3389/fendo.2024.1429567.
82. Huang Z, Meng FY, Lu LZ, et al. Calculus bovis inhibits M2 tumor-associated macrophage polarization via Wnt/β-catenin pathway modulation to suppress liver cancer. World J Gastroenterol. 2024;30(29):3511–33. https://doi.org/10.3748/wjg.v30.i29.3511.
83. Zhu Q, Li C, Wang K, et al. Phosphatase and tensin homolog-β-catenin signaling modulates regulatory T cells and inflammatory responses in mouse liver ischemia/reperfusion injury. Liver Transplant. 2017;23(6):813–25. https://doi.org/10.1002/lt.24735.
84. Shi J, Chi S, Xue J, Yang J, Li F, Liu X. Emerging role and therapeutic implication of Wnt signaling pathways in autoimmune diseases. J Immunol Res. 2016;2016:9392132. https://doi.org/10.1155/2016/9392132.
85. Bellavía S, Gallará R. Effect of photic stimuli on rat salivary glands. Role of sympathetic nervous system. Acta Odontologica Latinoamericana. 2000;13(1):3–19.
86. Pittenger MF, Discher DE, Péault BM, Phinney DG, Hare JM, Caplan AI. Mesenchymal stem cell perspective: cell biology to clinical progress. Npj Regen Med. 2019;4(1):22. https://doi.org/10.1038/s41536-019-0083-6.
87. Schnoell J, Jank BJ, Kadletz-Wanke L, et al. Protein expression of folate receptor alpha in adenoid cystic carcinoma of the head and neck. Onco Targets Ther. 2022;15:531–8. https://doi.org/10.2147/ott.s351500.
88. Wahl AM, Takano T, Su S, et al. Structural and functional analysis of salivary intercalated duct cells reveals a secretory phenotype. J Physiol. 2023;601(20):4539–56. https://doi.org/10.1113/jp285104.
89. Arner P. Regulation of adipose tissue lipolysis, importance for the metabolic syndrome. In: Östenson CG, Efendić S, Vranic M, editors. New concepts in the pathogenesis of NIDDM. Springer; 1993. p. 259–67.
90. Khezri MR, Yousefi K, Esmaeili A, Ghasemnejad-Berenji M. The role of ERK1/2 pathway in the pathophysiology of Alzheimer's disease: an overview and update on new developments. Cell Mol Neurobiol. 2023;43(1):177–91. https://doi.org/10.1007/s10571-022-01191-x.
91. Lin A, Dey D, Wong DTL, Nerlekar N. Perivascular adipose tissue and coronary atherosclerosis: from biology to imaging phenotyping. Curr Atherosclerosis Rep. 2019;21(12):47. https://doi.org/10.1007/s11883-019-0817-3.
92. Konieczny P, Xing Y, Sidhu I, et al. Interleukin-17 governs hypoxic adaptation of injured epithelium. Science (New York, NY). 2022;377(6602):eabf9302. https://doi.org/10.1126/science.abg9302.

Publisher's Note